Applied Energy 326 (2022) 119982

Contents lists available at ScienceDirect

Applied Energy

journal homepage: www.elsevier.com/locate/apenergy

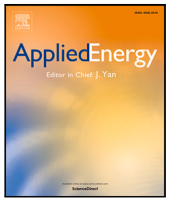

Optimal management of electric hotel loads in mild hybrid heavy duty truck

Somendra Pratap Singh [a,b], Athar Hanif [b], Qadeer Ahmed [a,b,*], Maarten Meijer [c], John Lahti [c]

[a] Department of Mechanical and Aerospace Engineering, The Ohio State University, OH 43210, USA
[b] Center for Automotive Research, The Ohio State University, OH 43212, USA
[c] PACCAR Technical Center, WA 98273, USA

ARTICLE INFO

Keywords:
Optimal energy management
Mild hybrid heavy-duty powertrain
Electric hotel loads

ABSTRACT

The problem of engine idling for heavy-duty trucks has been under study for decades with Auxiliary Power Units (APUs) and Truck Stop Electrification (TSE) as the most compelling solutions. With the electrification of trucks approaching feasibility in terms of cost-effective technology, hybridization offers another "degree of freedom" to tackle the problem. This work aims at exploiting a battery pack of a 48 V mild-hybrid heavy-duty truck to store sufficient onboard energy for powering the auxiliary loads during the hoteling. This problem is not trivial, as the battery packs typically cannot recover the entire energy required through regeneration alone; hence an optimal energy management strategy needs to be employed to charge the battery through the engine during drive operation. This strategy optimizes powertrain performances among the four modes: (i) Engine of Coasting (EOC), (ii) Regeneration by braking, (iii) Regeneration by engine, and (iv) engine idling. This paper presents the development of a Dynamic Programming (DP) framework that employs a multi-objective cost function to minimize the fuel consumption and maximize the regeneration using the above-mentioned four modes. A typical heavy-duty truck drive cycle is used to represent the drive phase, with mandatory hoteling stops as per regulations. A comprehensive powertrain model is developed using validated components' model. The DP employs two state variables: battery State-of-Charge (SOC) and engine mode, and three control inputs: (i) the engine ON–OFF state, (ii) clutch engagement state, and (iii) power request at the Electric Machine (EM) for calculating optimal SOC trajectory. The framework also tackles rapid engine ON–OFF scenarios to avoid the challenges associated with DP and the compromises in fuel cost with those approaches. Finally, the effectiveness of the proposed framework is tested for potential fuel savings on two different battery packs by performing the full cycle simulations. The results show 6.47% of fuel consumption reduction as compared to traditional APU-based heavy-duty truck.

1. Introduction

Over the years, the inefficient practice of idling heavy-duty trucks to power the cabin auxiliary loads has gained attention with solutions at the Original Equipment Manufacturer (OEM) level, personal or organizational levels. Moreover, a number of states have idling laws in place which limit the duration of idling through financial penalties for violations, such as California [1].

The statistics behind idling reduction technologies are best summarized in [2]'s report. Although the exact figures are difficult to obtain, it is estimated that the rest period idling contributed to annual fuel consumption of one billion gallons of fuel with a cost of approximately three billion US dollars. The term "rest-period idling" refers to the rest period of drivers lasting of up to eleven hours on weekdays. Based on the report it is estimated that approximately one million truck drivers rest overnight in the vehicle cab, leading to the staggering possibility of fuel savings lost to power the auxiliary loads during the rest period. Existing energy reduction technologies focus on fuel-powered APUs, rest stations, fuel-fired heaters, etc [2]. APUs are fuel-powered generator set which offers reduced power consumption and lower emissions compared to engine idle at a significant cost of equipment. Rest stations are alternatives that can either provide electrical energy to power the auxiliary loads or provide ducts to supply cooled/heated air during the rest period. While the solution seems lucrative with no investment on the truck and zero fuel consumption at the point of use, there may be initial investment costs and payback periods for rest-area owners that may last up to four years for 10% average occupancy (estimate from [2]). As an alternative to the existing methods, the presented approach aims at eliminating engine idling on electrified vehicles by ensuring a sufficient SOC of the battery at the end of a trip. This

* Corresponding author.
E-mail addresses: singh.1373@osu.edu (S.P. Singh), hanif.6@osu.edu (A. Hanif), ahmed.358@osu.edu (Q. Ahmed), Maarten.Meijer@PACCAR.com (M. Meijer), John.Lahti@PACCAR.com (J. Lahti).

https://doi.org/10.1016/j.apenergy.2022.119982
Received 15 April 2022; Received in revised form 4 August 2022; Accepted 12 September 2022
Available online 29 September 2022

requires two critical design decisions: (i) proper component sizing and architecture to store sufficient energy and ensure efficient regeneration, (ii) a proper energy management strategy to manage regeneration and engine-based battery charging. The above tasks are implemented on PACCAR's SuperTruck 2 program using realistic drive cycles and time-varying auxiliary loads through dynamic programming. While dynamic programming is not an online implementable control strategy in most cases [3,4], it would provide the framework to design an appropriate supervisory control strategy and compare it against the best possible solution returned by the DP solution.

Optimization-based Energy Management Systems (EMS) are offline strategies but especially effective in identifying trends for developing rule-based simplified strategies for online implementation. Lee et al. [5], Hegde et al. [6] calibrated a predefined torque split line based on DP results, while Wu et al. [7] implemented an A-ECMS strategy with equivalence factors returned through DP results. Even in sizing applications, Jung et al. [8] implemented a coupled approach of optimizing the component selection process by selecting components and implementing a DP approach for the best case fuel consumption. DP has also been exploited for multi-objective optimization as presented in [9,10], where fuel consumption and battery effective Ampere-hour (Ah) usage is minimized by ensuring the best fuel consumption with minimum battery wear. In the domain of heavy-duty trucks, Dellermann et al. [11] employed a DP simulation for a mild hybrid heavy-duty truck, and cabin temperature is also considered as a state other than the battery states. With a temperature tolerance of $+/-2$ °C, the strategy was able to attain a 10% benefit in fuel consumption with the P2.5 hybrid system.

The focus of heavy-duty truck electrification can be divided broadly into two main fields over the last few decades: (i) Accessory Electrification, and (ii) Powertrain Electrification [12]. Accessory electrification refers to system architectures where auxiliary loads are electrically managed instead of being mechanically coupled to the engine. With the additional flexibility of operating the auxiliary loads as per the load demand without engine-based constraints, efficiencies can be improved significantly for electrical components while removing loads that are managed inefficiently by the engine; affording further downsizing opportunities [13]. In the context of engine-idling, accessory electrification is the first step to ensure that components can be operated without dependence on the engine.

Surampudi et al. [14] details a comprehensive effort where parasitic loads on the engine are removed and are supported via a fuel cell APU connected to a 42 V electrified system. The energy improvements were substantial, for the HVAC system alone, the energy consumption of 4004 kJ dropped to 1761 kJ due to the electrified HVAC compressor. Moreover, it also highlights the reduction in total power requirement for auxiliary loads which means the APU can be downsized as compared to an APU based on mechanical power requirements as presented in [14,15]. More significant improvements can be seen in [16] which follows a similar approach to Surampudi et al. [14] in terms of component electrification with an APU. The simulation-based approach using ADVISOR is demonstrated in [17], and shows the fuel savings of 1300 gallons per year with a Solid Oxide Fuel Cell (SOFC) APU for a six-hour idle period. The study also gives insight into reduced power requirements from 2.7 kW average to 1.8 kW average and a drop of 2.1 kW from peak values through electrification. The idling numbers quoted for comparison are comparable to [2], ranging from 0.53 to 1.25 gallons per hour for engine idling. The power requirements for heavy-duty trucks were slightly different from [13], which reported an average of 2.2 kW for the HVAC compressor alone with a 50% duty cycle.

Surampudi et al. [18] reports further improvements for the electrified components using multiple control strategies. Three different sets of controllers were evaluated based on the logic for condenser fan and compressor speed with energy consumption ranging from 1228 kJ to 932 kJ for a 900 second approximate cycle. This work also reflects that the average power can be calculated to be 1.36 kW. These numbers for auxiliary loads and HVAC systems show a wide variation even among the category of heavy-duty vehicles. Campbell et al. [19] reports an average power requirement of 6.1 kW for HVAC alone in hybrid buses, simply because of large cabin volume and air loss over the operation cycle. Total auxiliary power consumption was reported at 11 kW on average in the absence of HVAC and 19.3 kW with HVAC. These numbers could be dropped to 7 kW and 13.3 kW respectively for HVAC OFF and HVAC ON cases by electrification alone.

In conclusion, the auxiliary power demands vary significantly depending on the class of vehicles, geographic location, and level of electrification. The summary of power requirements presented above will serve as a good estimate for full-cycle simulation results.

From the above discussion, it is clear that there is a true need for DP based framework for an optimal energy management system to evaluate the feasibility and benchmark hybrid powertrain performance in reducing the fuel costs for the hotel operation in a heavy-duty truck. The P2.5 architecture considered is limited in terms of energy flows since the EM would not be used for traction. Thus, this is a stark difference from conventional power-split hybrids which have been extensively studied in the literature for handling road loads only instead of hotel loads. Hence, considering both road and hotel loads will serve better representation of the typical drive cycle for benchmarking the fuel economy in heavy-duty trucks.

Keeping in view the aforementioned discussion, a DP-based optimal energy management strategy is proposed and developed to optimize the engine idling in the mild-hybrid heavy-duty trucks. This strategy maximizes the regeneration to charge the onboard battery pack while minimizing engine fuel consumption. This ensures sufficient onboard battery energy to meet the requirements of auxiliary loads during the hoteling. The proposed DP-based optimal energy management strategy is implemented using the realistic drive cycle to show its effectiveness.

The main contributions of the proposed work are:

- This study presents a modeling and control of a unique 48 V mild-hybrid P2.5 powertrain configuration where the onboard battery is used for managing the energy demands of hotel loads unlike in other electrified powertrain, where its primarily used for propulsion.
- A validated 0-D model for the powertrain is developed and its performance is optimized for a composite road load and hoteling load duty cycle for improved energy footprint and decreased parasitic loads on engine.
- An offline benchmark solution based on DP-framework is developed and evaluated for the design feasibility and optimization of the powertrain performance among the four operating modes: (i) Engine of Coasting (EOC), (ii) Regeneration by braking, (iii) Regeneration by engine, and (iv) engine idling. As compared to a traditional APU-based heavy-duty vehicle, a maximum of 6.47% of fuel consumption reduction is achieved.

The rest of the paper is organized as follows: Section 2 presents the mild-hybrid powertrain architecture for a heavy-duty truck and mathematical modeling of different powertrain components. Section 3 gives the details of the proposed optimization framework for a mild hybrid heavy-duty truck followed by the drive cycle processing and gear shift strategy in Section 4. Section 5 lays out the parameter identification and calibration methodology. Section 6 describes the vehicle specifications, details of simulations, proposed framework evaluation, and result discussion. Analysis using Composite "Short" cycle based on HHDDT Cruise cycle is presented in Section 7. Summary and concluding comments are detailed in Section 7.

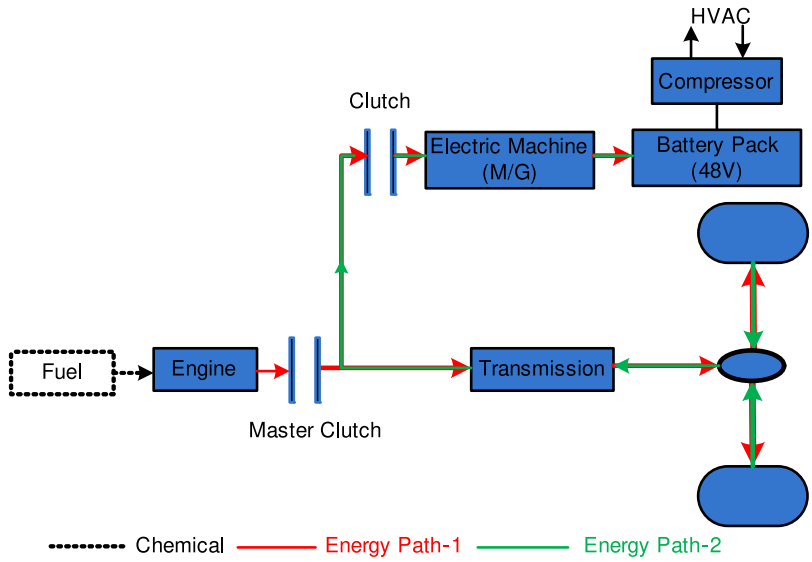

Fig. 1. Mild hybrid powertrain architecture for heavy duty truck (e.g. ST-2) from [20].

2. Mathematical modeling

2.1. Powertrain architecture

It is imperative to explain the overall architecture of the mild-hybrid heavy-duty truck under study. This would decide the constraints for the dynamic programming problem and the approach presented in the following sections.

A simplified mild-hybrid powertrain architecture for a heavy-duty truck is shown in Fig. 1. The engine supplied the required torque to the transmission through the master clutch. The transmission is an automatic gearbox with twelve gear ratios and the appropriate gear is selected through a predefined gear map with up-shift and down-shift hysteresis. It means that the up-shift conditions are not the same as the downshift conditions. The differential provides the final gear ratio and the output torque is provided to the wheels. It is clear that the architecture is a P2.5 hybrid, with the Electric Machine (EM) connected to the input shaft of the transmission. There exists a constant gear ratio between the transmission input shaft and the EM. Moreover, a clutch exists between the transmission and the EM. A transmission output shaft extends outwardly from the transmission and is driving connected with vehicle drive axles, usually by means of a prop shaft. Hence, torque can be transmitted in both directions but our present control strategy is to not use the EM as a motor (other than for engine starting). In the future, this work may consider motoring torque if the SOC is higher than the desired target. Therefore, EM cannot provide traction power to the wheels and can only be used for regenerating the energy from the wheels and the engine to charge the 48 V battery pack. The 48 V battery pack is used to meet the energy requirements of the hotel loads. Hence, it alters the problem formulation for the Dynamic Programming (DP) framework as compared to power split hybrids available in the literature [5,7,21,22]. The E-HVAC compressor is connected to the battery and has no mechanical connections to the powertrain (Fig. 1). This helps to generate the auxiliary load profile independent of the engine speed since there is no mechanical coupling.

The modeled mild-hybrid powertrain for the heavy-duty truck has four operating modes:

(M1) Engine of Coasting (EOC): defueling the engine while the vehicle is moving based on vehicle operating conditions and routes rotational energy.

(M2) Regeneration from braking: while the vehicle is moving and depending on the route.

(M3) Regeneration from engine: if energy from the braking is not sufficient to achieve the desired SOC of onboard battery pack during the drive phase.

(M4) Engine idling: operates the engine while stopped to maintain the accessory functions such as 'hotel loads' if the onboard battery pack has SOC less than 20%.

2.2. Vehicle longitudinal model

The DP framework assumed that the velocity profile is not violated. Hence, a longitudinal model similar to the one used for gear profile estimation is used for calculating the propulsion torque requirement from the tractive force.

$$\begin{aligned} F_{total} &= F_{inertia} + F_{aerodynamic} + F_{road} + F_{grade} \\ &= m\frac{dv}{dt} + \frac{1}{2}\rho C_d A_{frontal} v^2 + C_r mgcos(\alpha) + mgsin(\alpha) \end{aligned} \tag{1}$$

where F_{total} is total propulsion force, ρ is air density, C_d is drag coefficient, A_f is frontal area, v is vehicle velocity, m is vehicle mass, g is gravitational acceleration, α is grade angle and C_r is rolling friction coefficient.

These correlations can be then used to evaluate the power and torque at the wheels and given as:

$$T_w = r_w F_{total} \tag{2}$$

$$P_w = F_w v = T_w \omega_w \tag{3}$$

where T_w is torque at wheel, r_w is wheel radius, P_w is power at wheel, v is vehicle longitudinal velocity, ω_w is wheel rotational speed.

2.3. Gearbox

The system employs a 12 speed AMT with a final reduction using a differential. The gearbox input shaft torque is determined as:

$$T_g = \frac{T_w}{\eta_g \gamma_i \gamma_f} \tag{4}$$

$$T_g = \frac{T_w \eta_g}{\gamma_i \gamma_f} \tag{5}$$

where T_w is torque at wheel, T_g is torque at transmission input/engine output shaft, γ_i is gear ratio γ_f is the final drive reduction and η_g is overall transmission efficiency including final drive. η_g is constant in

all cases at 95%. Eqs. (4) and (5) are for positive torque and negative torque, respectively.

The clutch is modeled as discrete event an ON–OFF switch with two discrete possible values with discrete input as control variable. This is explained in Section 3 (Control Inputs). The purpose of the clutch is to ensure the correct behavior of engine and clutch while positive tractive force and is used for defining mode in-feasibility constraints as shown in Section 3. An 'ON' or '1' position shows that the engine is disengaged with the transmission and a value of 'OFF' or '0' represents an engaged position. There are no dynamics or fuel costs associated with clutch due to the following reasons:

- The transients associated with clutch shifting are high frequency events and they have minimal impact on the fuel economy.
- Moreover, the base cycle has minimal gearshifts due to being a cruise cycle, the impact on fuel consumption with shifting is negligible.

With these assumptions, the model shows good agreement in terms of fuel consumption with the manufacturer data for the cycle.

2.4. Engine

The engine model is implemented as 2D lookup table from manufacturer data, similar to [9,23]. It calculates the fuel flow rate ($\dot{m}_f$) based on the operating conditions of the engine (T_{eng} and ω_{eng}).

$$\dot{m}_f = f(T_{eng}, \omega_{eng}) \tag{6}$$

Component constraints on the engine are expressed as:

$$0 < T_{eng} < T_{max}(\omega_{eng}) \tag{7}$$

$$RPM_{ENG,min} < \omega_{eng}\frac{30}{\pi} < RPM_{ENG,max} \tag{8}$$

where $RPM_{ENG,min}$ and $RPM_{ENG,max}$ are the engine speed limits in Revolution Per Minute (RPM).

2.5. Electric machine map

The EM is also implemented as a 2D lookup table. The table relates the operating points of the EM, the torque T_{EM} and speed ω_{EM} with the motor energy efficiency η_{EM}.

$$\eta_{EM} = f(T_{EM}, \omega_{EM}) \tag{9}$$

The motor torque and speed are further constrained by physical limits expressed as:

$$0 < T_{EM} < T_{max}(\omega_{EM}) \tag{10}$$

$$0 < \omega_{EM}\frac{30}{\pi} < RPM_{EM,max} \tag{11}$$

where 0 and $RPM_{EM,max}$ are the minimum and maximum EM speed in rotations per minute. A point to consider is that the EM always operates in one quadrant, unlike conventional power-split hybrids. The positive torque in this case is for generating. The torque T_{EM} is appropriately modified in its sign to account for this limitation.

Due to the operation in only one quadrant, the electric power output from the EM can be expressed as:

$$P_{EM} = T_{EM}\omega_{EM}\eta_{EM} \tag{12}$$

where η_{EM} is a function of the torque T_{EM} and speed ω_{EM}.

2.6. Battery model

The battery model is implemented using a zeroth order battery [23–26]. This model condenses a cell to an Electro-motive force (EMF) source in series with a resistance. The resistance and EMF following a nonlinear relationship with factors such as State-of-Charge (SOC), temperature etc. For ST-2, the mathematical formulation for the battery pack is represented as:

$$R_{cell} = f(SOC, sgn(I)) \tag{13}$$

$$V_{oc} = f(SOC) \tag{14}$$

where R_{cell} is the cell resistance, SOC is state-of-charge, I is cell current, V_{oc} is open circuit voltage. These nonlinear relationships are implemented using one-dimensional (1-D) lookup tables in the simulation. The change in the SOC state is based on coulomb counting which requires a calculation for current. These calculations are based on solving the quadratic equation as given:

$$I = \frac{V_{oc} - \sqrt{V_{oc}^2 - 4RP_b}}{2R} \tag{15}$$

$$SOC_{t+1} = SOC_t + \frac{\eta_b I}{Q} \tag{16}$$

where I, V_{oc}, R, η_b, Q and P_b represent the pack current, pack open-circuit voltage, pack resistance, efficiency, pack capacity and pack power respectively. These values are either inputs or derived from cell level values based on the number of cells in series and parallel. The discharge efficiency is 99% and the charging efficiency is 95%.

3. Proposed optimization framework for heavy duty truck

3.1. Problem statement

Mild hybrid power-train configuration is deployed in heavy duty trucks (i.e. SuperTruck 2) to only fulfill the power needs of the hotel loads. The aforementioned configuration is not adopted for the traction purposes. The 48V on board battery pack is used to supply the hotel loads. Therefore, the objective is to minimize the fuel consumption keeping in view the eHVAC and hotel loads and maximize the regeneration to meet the power requirements for the hotel loads without engine idling over the entire period of hotel operation.

Therefore, there is a genuine need for the optimization framework to achieve the solution for the above mentioned problem. The approach taken in this manuscript is to implement a DP based optimization framework to identify the optimal control strategy for minimizing fuel consumption over the entire cycle which includes the drive and hotel phases. Optimization based energy management systems have a crucial role despite their inability to be implemented online in most cases [3,4]. Fig. 2 depicts the details of proposed dynamic programming based energy management system for heavy duty truck keeping in mind the unique powertrain configuration of SuperTruck-2.

3.1.1. Assumptions

The following assumptions are taken for the realization of the DP approach:

1. The vehicle meets the traction torque demand at all times. This eliminates the necessity to add velocity as a state variable and simplifies the formulation drastically.
2. The physical component constraints are not violated at any point. To achieve the minimal intervention with the gear map for drivability concerns, the gear profile presented in Fig. 6 is strictly followed.
3. The framework does not account for emission or other constraints. In this manuscript, only the global fuel consumption is optimized while operating the EM at high efficiency zones and minimizing the number of start and stops.

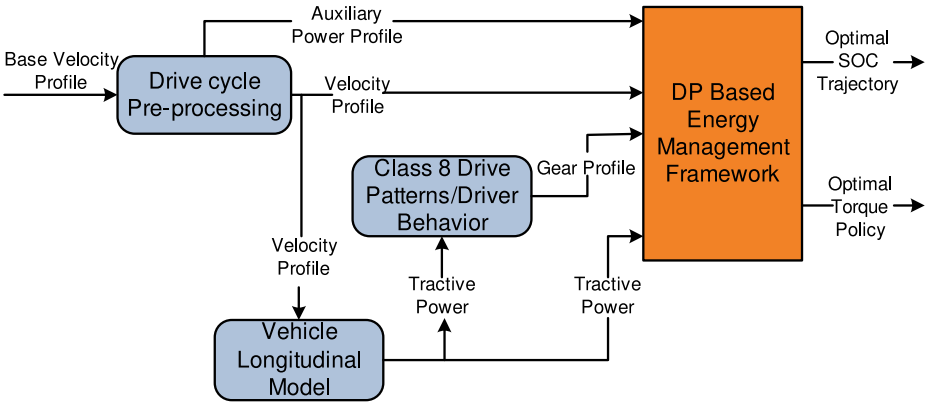

Fig. 2. Dynamic Programming based energy management system for heavy duty truck.

3.2. Cost function

The multi-objective cost function is formulated to achieve the objectives for this work and is expressed as Eq. (17). It weighs multiple targets through user defined weighing parameters.

$$J = \left[\alpha\left(\frac{\dot{mi}_f}{\dot{m}_{f,max}}\right) + \beta\left(1 - \frac{T_{EM}\omega_{EM}\eta_{EM}}{P_{EMmax}}\right) + (\dot{m_{f,ss}})\right] \tag{17}$$

$$\alpha + \beta = 1 \tag{18}$$

where α, β are weighing coefficients for fuel cost and regeneration in-efficiency.

The term $\alpha\left(\frac{\dot{mi}_f}{\dot{m}_{f,max}}\right)$ reflects the normalized fuel consumption with a weighing factor α. This normalization enables the researcher to make a multi-objective function with the ability to skew the results as needed. The term $(\beta\left(1 - \frac{T_{EM}\omega_{EM}\eta_{EM}}{P_{EMmax}}\right))$ represents the regeneration in-efficiency and is a term that enables the researcher to operate the EM at points which results in a high energy absorption. The term $(\dot{m_{f,ss}})$ is a user imposed start–stop cost which is implemented only when the engine is switches ON from and OFF position and when the vehicle is in neutral. The implementation of this cost only during stops is to allow the engine to coast in OFF position freely while in drive phase.

3.3. Control inputs

Since the EM is not able to share a traction load, a power split (found in conventional Hybrid Electric Vehicle (HEV) literature) is not applicable to the problem statement. Due to the limited energy flow paths, the choice of control inputs is:

$$u(t) = \{T_{EM}, s_{clutch}, s_{eng}\} \tag{19}$$

- T_{EM} is the torque of the electric machine. The speed of the electric machine is determined by the engine speed. Therefore, to define the power absorption, EM torque is required which is now a control input.
- s_{clutch} is a discrete variable with a value of either 0 or 1. This represents the engagement status of the clutch. A value of 0 means the engine is connected to the transmission and a value of 1 indicates that the engine is disengaged from the transmission.
- s_{eng} is another discrete variable with a value of 0 or 1. It indicates the status of the engine; i.e., whether the engine is OFF (0) or ON (1).

3.4. State variables

The three state variables are the battery SOC, the engine mode and clutch state. At every instant, the choice of the control inputs affect the battery pack's SOC. The engine state is a discrete variable and is fundamentally the state of the engine (0 or 1) at the previous time-step. This enables the framework to compare the control input for the engine at the current time-step and decide whether or not an engine start–stop penalty has to be applied.

3.5. Constraints

The constraints for the DP formulation can be segmented into three main sub-sections.

3.5.1. State constraints

The SOC of the system, by design is not allowed to cross a value of 0.9 or drop below 0.2. Therefore,

$$SOC \in [0.2, 0.9] \tag{20}$$

The engine state is a discrete variable and is determined directly by the engine state in the previous time-step. Hence it does not require an explicit constraint.

3.5.2. Component constraints

These refer to the physical limitations of all powertrain components. Thus, for the engine:

$$0 < T_{eng} < T_{max}(\omega_{eng}) \tag{21}$$

$$RPM_{ENG,min} < \omega_{eng}\frac{30}{\pi} < RPM_{ENG,max} \tag{22}$$

On similar lines, there are torque and speed constraints on the electric machine defined as:

$$0 < T_{EM} < T_{EM}(\omega_{EM}) \tag{23}$$

$$0 < \omega_{EM}\frac{30}{\pi} < RPM_{EM,max} \tag{24}$$

Lastly, the battery is not allowed to violate the peak charging or discharging current values. These current limits depend on the number of parallel cells.

For the battery pack-1 (14.256 kWh),

$$0 < |I_{battery,dis}| < I_{max} \tag{25}$$

$$0 < |I_{battery,ch}| < I_{max} \tag{26}$$

For battery pack-2 (21.384 kWh), the limitations are modified to:

$$0 < |I_{battery,dis}| < I_{max} \tag{27}$$

$$0 < |I_{battery,ch}| < I_{max} \tag{28}$$

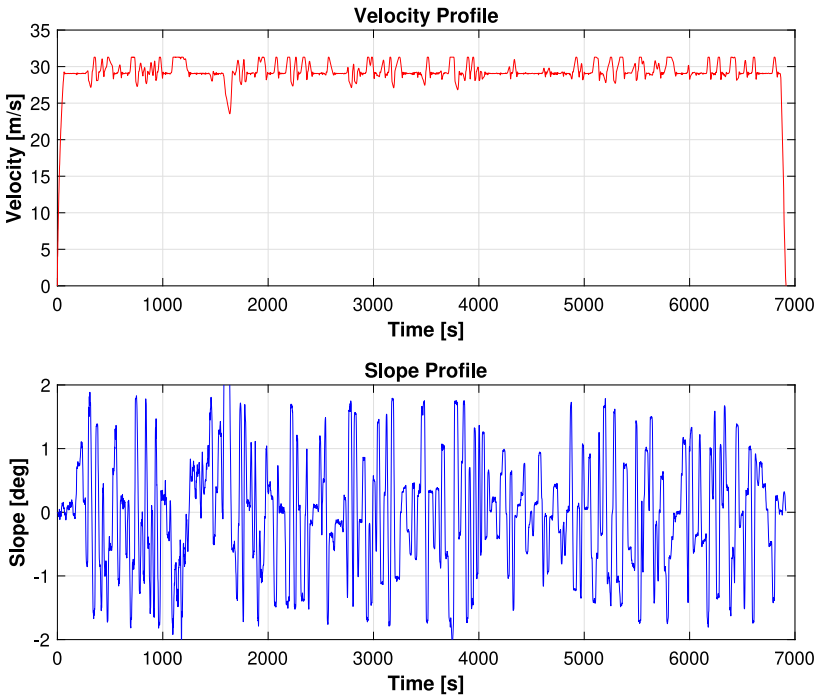

Fig. 3. Base velocity profile for heavy duty truck (e.g. ST2).

For both the packs, the constraint on voltages remains the same, thus:

$$V_{min} < V_{cell} < V_{max} \tag{29}$$

The above constraint is based on a single cell and are modified based on the cells in series for both battery pack-1 and battery pack-2 configurations.

3.5.3. Mode in-feasibility constraints

The DPM function is implemented in three distinct segments based on the torque request at the wheels. At all these three conditions, it is necessary to define a set of constraints such that the underlying assumptions are not violated. Fundamentally, in the traction phase, it is not allowed to disengage the clutch or switch the engine OFF. These situations might be deemed allowable if not explicitly constrained as the DP would only focus on minimizing the fuel. Thus, to ensure that the drive cycle is followed correctly, following two mode in-feasibility constraints are adopted.

- Case 1: $T_w > 0$: With a positive traction torque requirement, clutch disengagement and engine switch OFF modes are not allowed.

$$I_{mode} = (T_w > 0)\&(s_{clutch} == 1) + (T_w > 0)\&(s_{eng} == 0) \tag{30}$$

  This condition ensures that the clutch is not disengaged and the engine is always ON while propulsion.
- Case 2: $T_w < 0$: With a negative torque, the maximum allowed power request at EM should not exceed the power available at the wheel, hence:

$$I_{mode} = (T_w < 0)\&(|P_{EM}| > |0.95 * P_{wheel}|) \tag{31}$$

4. Drive cycle processing and gear shifting algorithm

Drive cycle pre-processing and gear shift strategy are crucial for the proposed DP based optimal energy management system as shown in Fig. 2.

4.1. Cycle inputs

A heavy duty truck drive cycle differs significantly from a conventional drive cycle. Specifically, the driving behavior over an entire day becomes the point of interest since the average distance traveled per day is over 600 miles for such vehicles. To develop a composite cycle, a base cycle shared by the manufacturer on a highway drive was utilized and presented in Fig. 3. The composite cycle is developed by repetitions of the base cycle shown in Fig. 3 with two short breaks (i.e. 0.5 h each) in between and one long idle period (i.e. 10 hours) representing an overnight resting situation. The composite cycle is shown in Fig. 4. It is based on driver behavior data compiled by the manufacturer. The drive phase is approximately 10.5 h.

With the knowledge of the composite drive cycle, a composite auxiliary load cycle is developed and shown in Fig. 5. The drive phase has a nominal accessory load of 7kW which is based on approximations from literature (non HVAC drive load from [19] for electrified systems since HVAC power consumption for heavy duty truck (e.g. ST2) is relatively lower) and manufacturer specifications. The nominal auxiliary load while idling varies from 1 kW to 2.5 kW in steps of 500 W. There are four different cases which form an envelope of possible nominal auxiliary loads. The nominal loads also reflect the variance in literature when it comes to HVAC loads [13,18,19]. Moreover, additional loads of 500 W or 800 W (such as lights, microwave oven, etc. operations) are added at different parts of the short or long breaks to the nominal loads while stops. With the absence of accurate hotel loads, these driver patterns and subsequent composite drive cycles show the close representations of hotel loads for an aggressive operation. This forms the inputs to the development of DP framework to minimize the fuel consumption and maximize the regeneration to meet the energy consumption for the hotel loads over the entire period of operation.

4.2. Gear selection pre-processing

Fig. 6 shows the gear map with the down-shift and up-shift hysteresis. Conventional gear selection maps are based on engine torque request and vehicle speed. However in heavy duty truck (e.g. ST2), the gear map is based upon the vehicle velocity and the power requirement

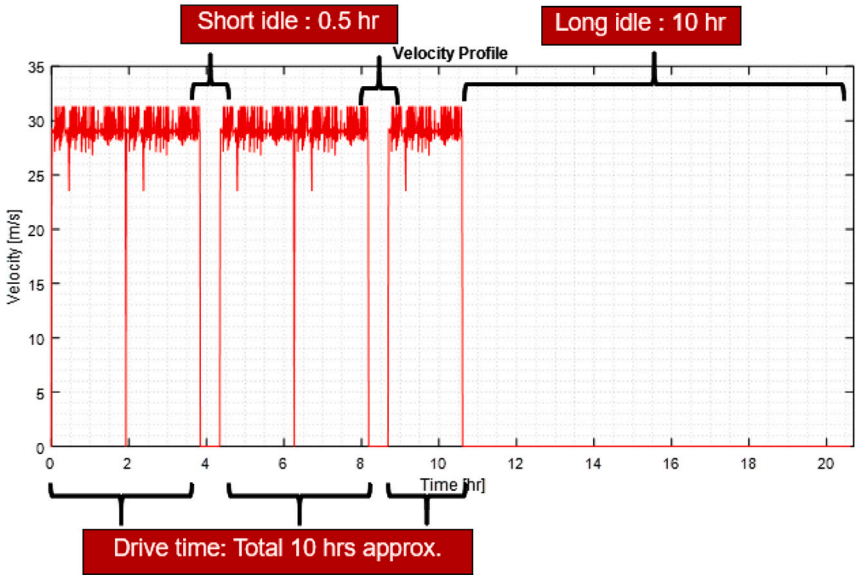

Fig. 4. Composite drive cycle for heavy duty truck (e.g. ST2).

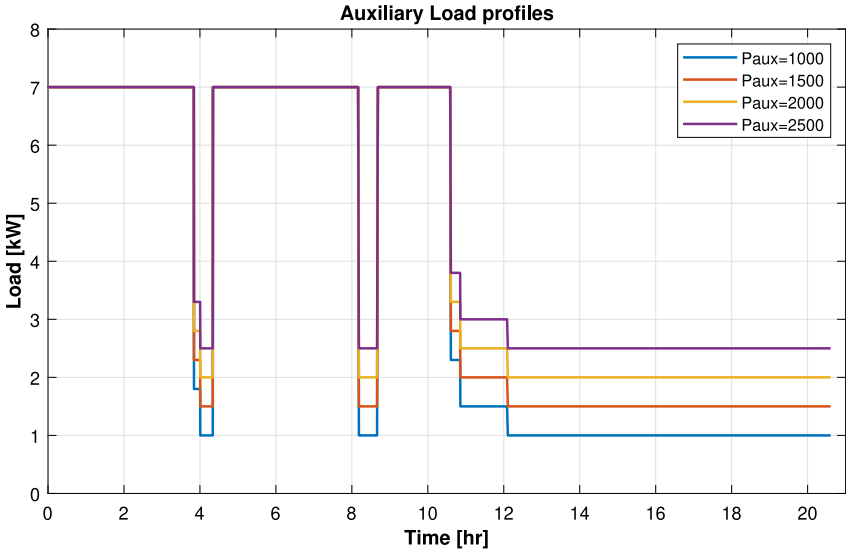

Fig. 5. Composite auxiliary load cycle for heavy duty truck (e.g. ST2).

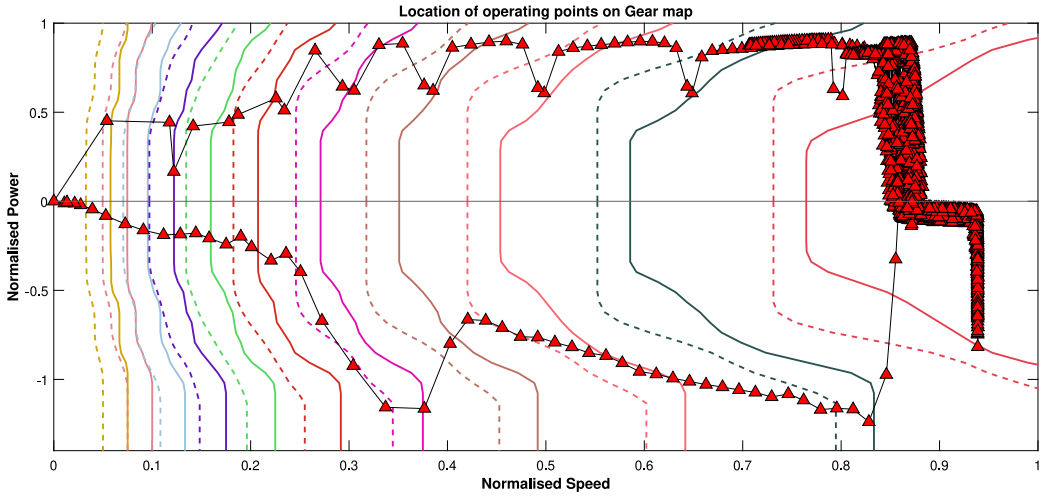

Fig. 6. Gear shift map with the down-shift and up-shift hysteresis.

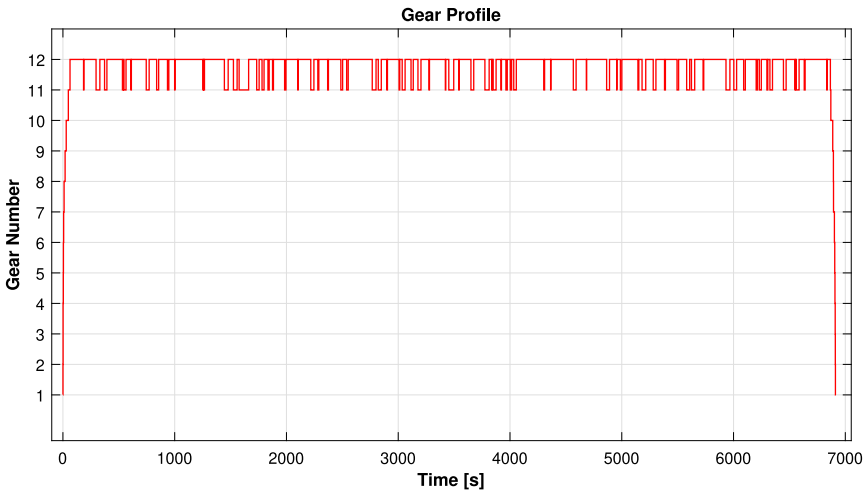

Fig. 7. Gear map for the velocity and altitude profile.

at the engine. A dedicated velocity and altitude profile are provided by the manufacturer which are then used for tractive force at the engine using the formulation presented in Eq. (32):

$$F_{wheel} = [\underbrace{\frac{1}{2}\rho_{air} C_d A_f v^2}_{\text{Aerodynamic}} + \underbrace{mgC_r cos\alpha_g}_{\text{Rolling}} + \underbrace{mgsin\alpha_g}_{\text{Grade}} + \underbrace{m\frac{dv}{dt}}_{\text{Inertia}}] \tag{32}$$

where ρ_{air} is air density, C_d is drag coefficient, A_f is frontal area, v is vehicle velocity, m is vehicle mass, g is gravitational acceleration, α_g is grade angle and C_r is rolling friction coefficient. The values of C_d, A_f, M, and C_r are specific for ST-2 from the manufacturer, whereas the slope α and velocity v are determined from the drive cycle and altitude data.

4.2.1. Algorithm for gear shift identification

The gear shift identification was done in sequential way (i.e. the algorithm to determine the appropriate gear requires the gear information at the previous time-step to determine the up-shift and down-shift line). Following steps are adopted for the gear shift identification.

1. Identify velocities at current and next time-step v_t and v_{t+1} and power requirements P_t, and P_{t+1}.
2. Determine the appropriate up-shift and down-shift line. An up-shift and down-shift line is an array of values relating power to velocity.
3. Find the threshold velocities v_{th1}, and v_{th2}; these are points on the up-shift/down-shift line for the power requirements P_t, and P_{t+1}.
4. The conditions for up-shift and down-shift are summarized below:

$$Upshift = v_t < v_{th1} AND v_{t+1} > v_{th1} \tag{33}$$

$$Downshift = v_t > v_{th2} AND v_{t+1} < v_{th2} \tag{34}$$

The resulting gear map for the velocity and altitude profile is shown in Fig. 7.

The engine operating points highlight the feasibility of the above gear profile and verify the fuel consumption error to be under 3.5%. Fig. 8 outlined the flow of steps adopted in the proposed scheme for the energy management system.

5. Parameter identification/calibration

The choice of cost function makes it necessary to decide the values of two parameters, (α) and ($m_{f,ss}$). These parameters were found using two studies which vary the parameters between extremes and analyze the results to draw a conclusion.

5.1. Weight parameter

Eq. (17) is a normalized cost function with two primary parameters: (i) the fuel consumption and (ii) efficiency of electric machine during regeneration. The parameter α is the biasing parameter that decides if the optimization prioritizes fuel consumption or electric machine efficiency. It is expected that as the value of α is increased, the fuel consumption during the drive cycle will drop at the cost of electric efficiency. At the extremes, it is also clear that the benefit of an α value near 0 or at 1 will stagnate the benefits of one of the objectives and in between these two extremes will be a trade-off point of interest.

Initially, a coarse run was simulated and it was found that beyond an α value of 0.8, the gradient of fuel consumption undergoes significant changes. With a finer simulation sweep of α, it was observed that the rate of decline of fuel consumption is significant in this region. This behavior is expected, as an increase in α will prioritize the fuel consumption more aggressively as shown in Fig. 9. However, beyond a value of 0.9 there is no noticeable increase in fuel economy as the gradient stagnates, but the electric machine efficiency still shows a rapid decline (shown in Fig. 12) since the algorithm will prioritize even a minimal increase in fuel economy at the cost of significant drop in electric machine efficiency. This region is therefore critical to the bias factor selection and it is clear that a value beyond $0.88 - 0.9$ will yield no tangible increase in fuel economy but will increase the potential of electric machine inefficiency. A value of 0.88 is therefore decided as the bias factor to prioritize fuel consumption (beyond which fuel consumption improvement is minimal) without massive compromises with motor operating efficiency.

5.2. Start–stop cost

In the most fundamental implementation, the start–stop cost is a fuel penalty incurred when the engine switches ON from an OFF condition and has the potential to limit the number of engine start–stop over the complete drive cycle. While this is a desirable trait for the hotel phase, a start–stop cost in the drive phase leads to an increased in the fuel consumption. From the powertrain characteristics, it is possible to switch the engine OFF during a negative torque request at the wheels. This is a condition referred as Engine OFF Coasting (EOC). As the start–stop cost is increased, it becomes infeasible for the DP to switch the engine OFF for short duration and thus the opportunities for EOC are lost. This is shown in Fig. 10. Fig. 10 shows that as the fuel cost increases to 5 grams, the EOC loss is maximized and stagnates. The increased fuel consumption is shown in Fig. 11 and shows the same stagnation at 5 grams.

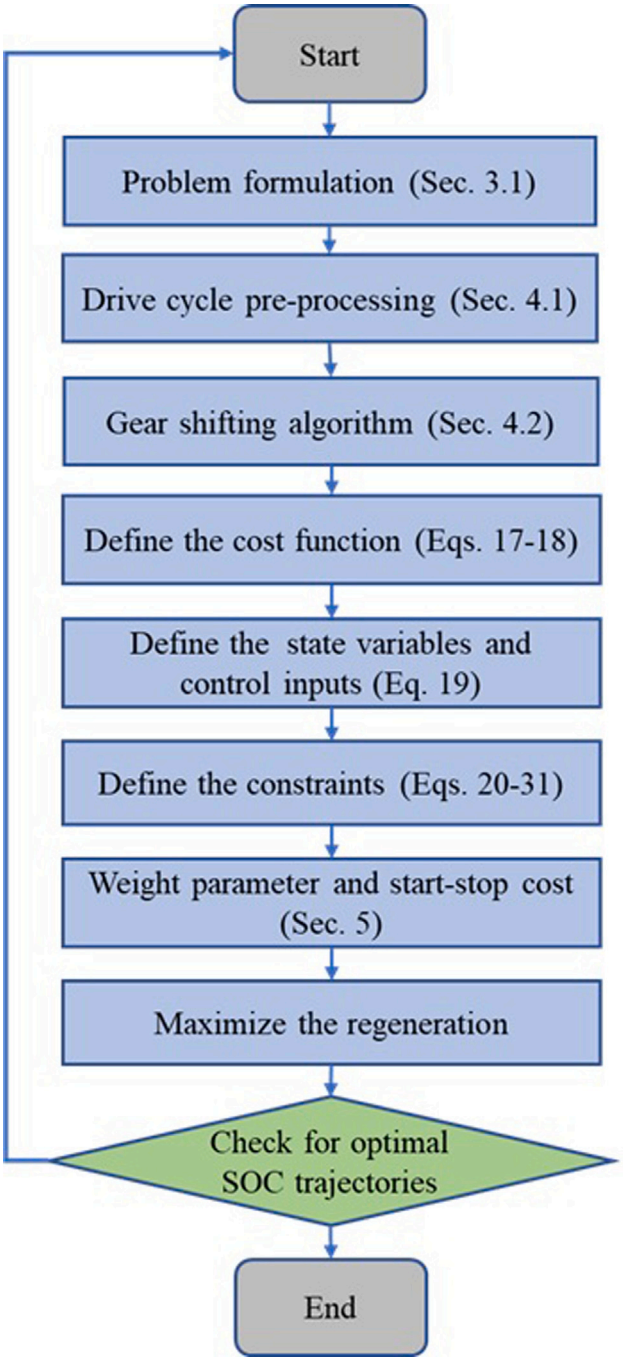

Fig. 8. Flow diagram for the proposed scheme.

To overcome this EOC loss, the penalty is implemented only during the idle phase and is conditioned on the transmission gear being neutral. This implies that the system is free to enter EOC even for a small duration but is limited by the DP framework during the hotel phase to limit the number of engine start–stop.

Figs. 13 and 14 show that if the idle start–stop cost is implemented only during vehicle stops (hotel period), the penalty on fuel consumption is minimal. However, it is a powerful tool to control the number of start–stop as seen in Fig. 14. For the full cycle evaluation, the results are presented with a start–stop cost of 5 gram as the number of start–stop is constant beyond this value.

6. Performance evaluation

This section will elaborates the SOC trajectories for different loads, SOC based torque request results and battery power segment simulation results. The term "Segment" refers to a specific part of the drive cycle. These segments help to quantify the outcomes of this work in Section 6. The three segments are shown in Fig. 15 and can be describes simply as:

- Segment 1: Start of Drive cycle to the beginning of first short idle period (representing a short break during the trip in Fig. 4). This is composed of 2 repetitions of the base drive cycle.
- Segment 2: End of first short idle period to the beginning of the second short idle period. Similar to Segment 1, it is also composed of 2 repetitions of the base drive cycle.
- Segment 3: End of second short hoteling period to the beginning of the long-overnight hoteling period. This segment only consists of 1 base drive cycle.

The three segments represent the only possible opportunities for SOC regeneration and the time in the drive cycle other than the three segments are idling periods with accessory loads.

In evaluation of proposed algorithm, EOC mode (M1) is enforced in the DP algorithm as a condition which is true at every instance when the torque requirement at the wheel is 0. The correlation of fuel consumption, which resulted in a deviation of only 3.5% from testing data validates the assumption of embedding this in the calculations.

6.1. SOC trajectories

Fig. 16 compares the SOC profiles from the DP solution for the four different auxiliary loads ranging from 1 kW to 2.5 kW and for the two different battery packs (i.e. battery pack-1 (14.256 kWh), and battery pack-2 (21.384 kWh)). Since the pack capacities are different, the analysis is split based on the pack configuration. For the battery pack-1, it is concluded that the pack is incapable of supporting a hotel load overnight without an idling phase (M4). Due to limited capacity, this pack has a peak charging time through idling for approximately 1.9 h. After the evaluation, it is also concluded that even though the velocity profile is based on a repetition of a base profile, the SOC behavior in these repeated segments is visibly different. In case of the battery pack-1, all systems reach an eventual SOC of 90% at the end of the total drive phase, however the difference in the first segment is maximum and least in the last segment.

The battery pack-2 takes advantage of the increased pack capacity and can support a 1kW nominal hotel load profile without an idle period. The remaining three cases require at least one idling phase to sustain the loads as observe in the battery pack-1. Though the segment wise differences in SOC profiles are less pronounced compared to the battery pack-1. It is vivid that the segment-1 showing the maximum differences which is fairly non-existent in the 3^{rd} segment.

6.2. Torque request-SOC based results

Fig. 17 shows the incremental torque request on the engine for battery regeneration as a function of SOC. This plot essentially condenses the time-series information as already clear from Fig. 16 that the SOC is following an increasing trend with time. The behavior of the battery pack-1 is strikingly different from the battery pack-2. The battery pack-1 shows a dramatic variation in the torque request from the engine for SOC below 50%, which coincide with the first segment of the drive cycle. In this region, the torque requests are influenced by the auxiliary load values for the hotel period. The requests peak at about 110 N.m and show a decreasing trend as the SOC approaches the 50% mark. From 50% to approximately 70%, the torque request at the engine is under 40 N.m with no visible trend (neither increasing or decreasing). As the third drive segment starts, the torque request on the engine overlaps for all load cases and increases in trend to achieve a 90% end SOC. The battery pack-2 is fairly consistent in terms of torque request to the engine upto 70% SOC, beyond which it exhibits a similar behavior as the battery pack-1 with the only exception being the 1kW case as it does not require an end SOC of 90%.

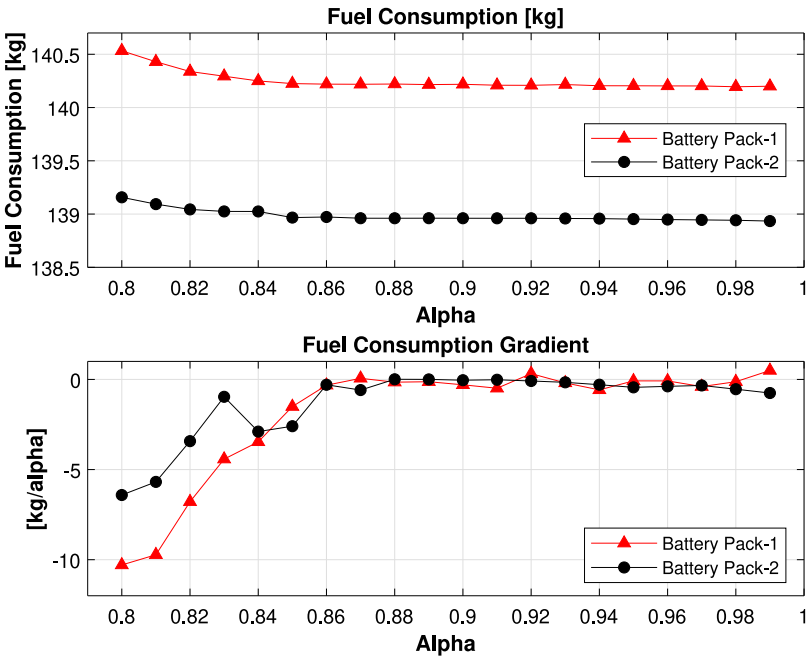

Fig. 9. Impact of parameter α on fuel consumption.

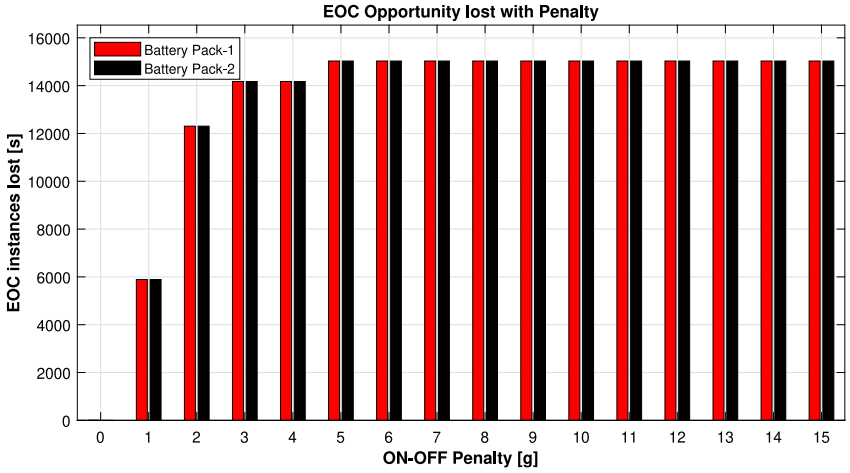

Fig. 10. Impact of start–stop cost on number of start and stop.

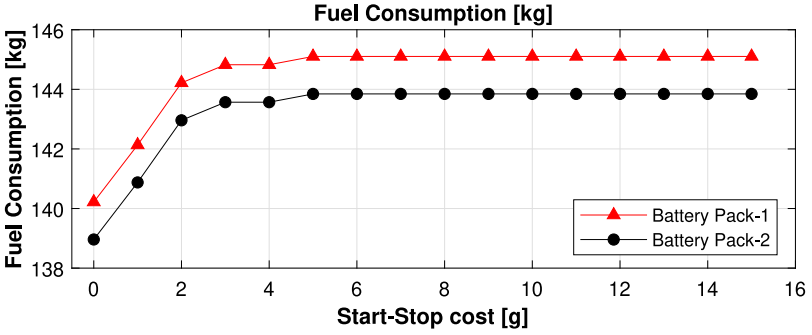

Fig. 11. Impact of an un-conditional start–stop cost on fuel consumption.

6.3. Battery power-segment based results

A torque request at the engine is not the absolute reason for the increase in SOC since it could only be supporting the drive auxiliary load of 7 kW. To better demonstrate the opportunities for SOC increase, Fig. 18 present the regeneration from engine mode (M3) for three segment over the entire drive cycle. The operating points, shown in Fig. 18, are the points where the battery power input is negative, or

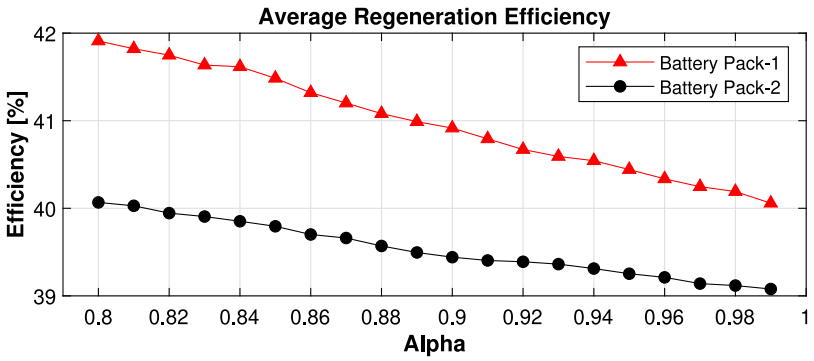

Fig. 12. Regeneration efficiency with weight parameters.

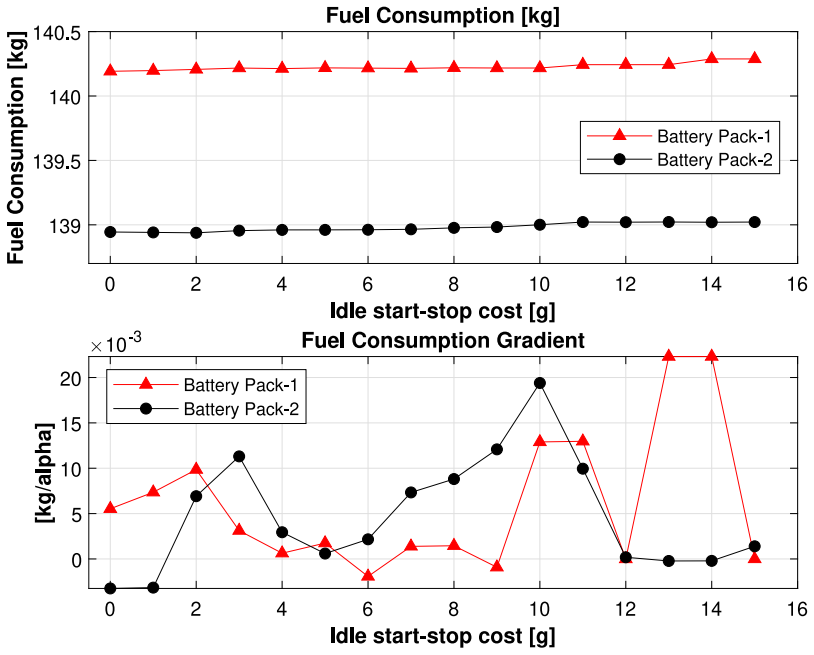

Fig. 13. Impact of hotel operation: only start–stop cost on fuel consumption.

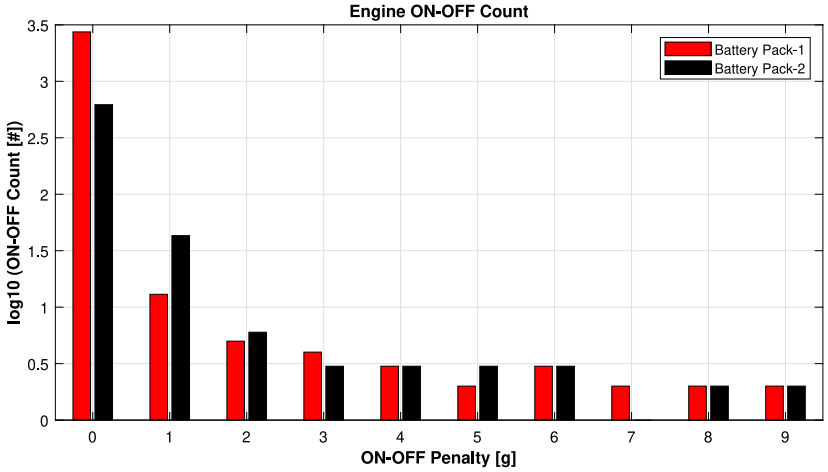

Fig. 14. Impact of hotel operation: only start–stop cost on number of start–stop.

the charging phase of the battery during positive torque request at the wheel. By convention, a positive power is a power draw from the battery. Similarly, Fig. 19 depict the regeneration from braking mode (M2) for three segment for the complete drive cycle. The operating points, shown in Fig. 19, present that charging phase of the battery pack is accomplished during positive torque request at the wheel.

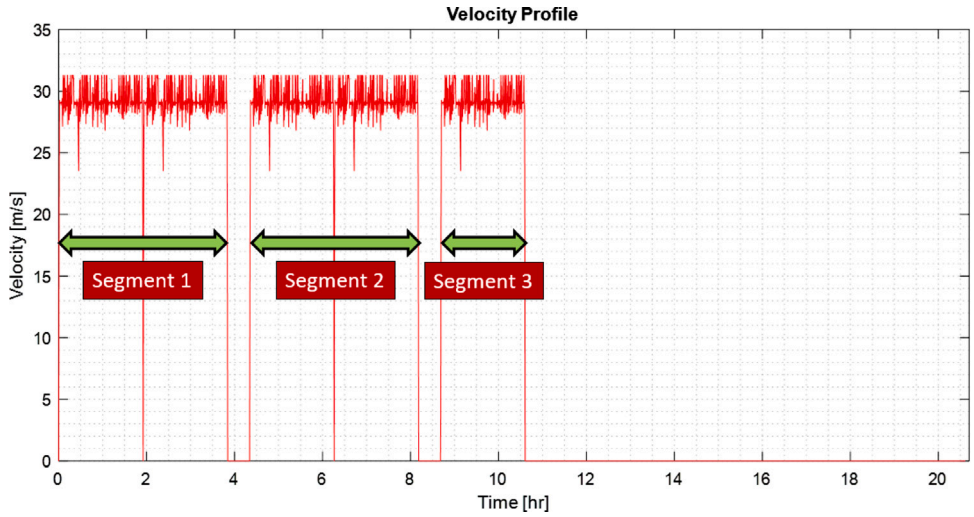

Fig. 15. Segments in the composite velocity cycle.

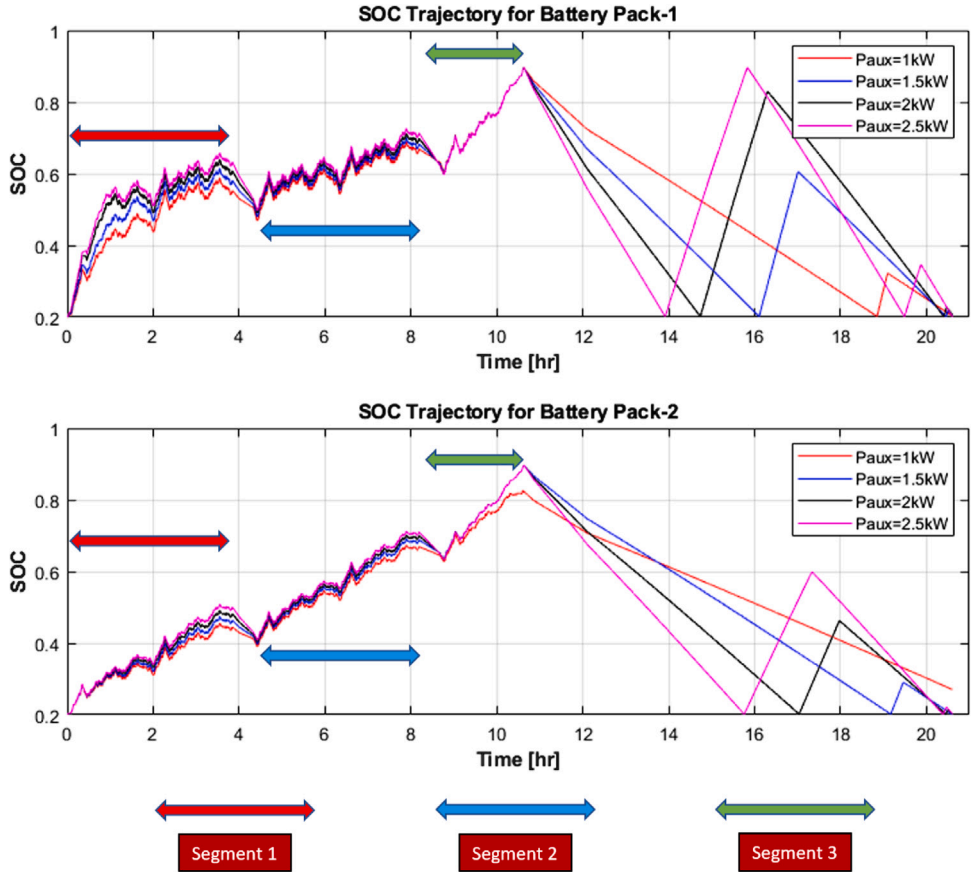

Fig. 16. State-of-Charge (SOC) Trajectories for composite velocity cycle.

During a positive torque request, it is observed that for the battery pack-1 the engine provides energy input into the battery during multiple phases of the first drive segment and it represents the M3 operating mode. As the SOC converges to the 0.5 – 0.6 SOC band, the engine torque offsets the power request due to auxiliary loads and thus the net flow is under 7kW for multiple instances. During the last segment, the engine again provides power to reach the end SOC target (M3 operating mode). In case of the battery pack-2, however, the engine primarily offsets the auxiliary requirements during the drive phase with engine based SOC gain only in the last segment. Fig. 19 shows that the major SOC gain takes place during brake based regeneration at times of negative torque request. Thus, the mild hybrid setup primarily exploits the energy available during regeneration, with the engine required to only offset the drive phase demand in most instances.

6.4. EM operating points

The EM operating points are only shown for qualitative analysis. Figs. 20 and 21 show the operating point comparison for the both battery packs for 1 kW and 2.5 kW hotel load cases. One system

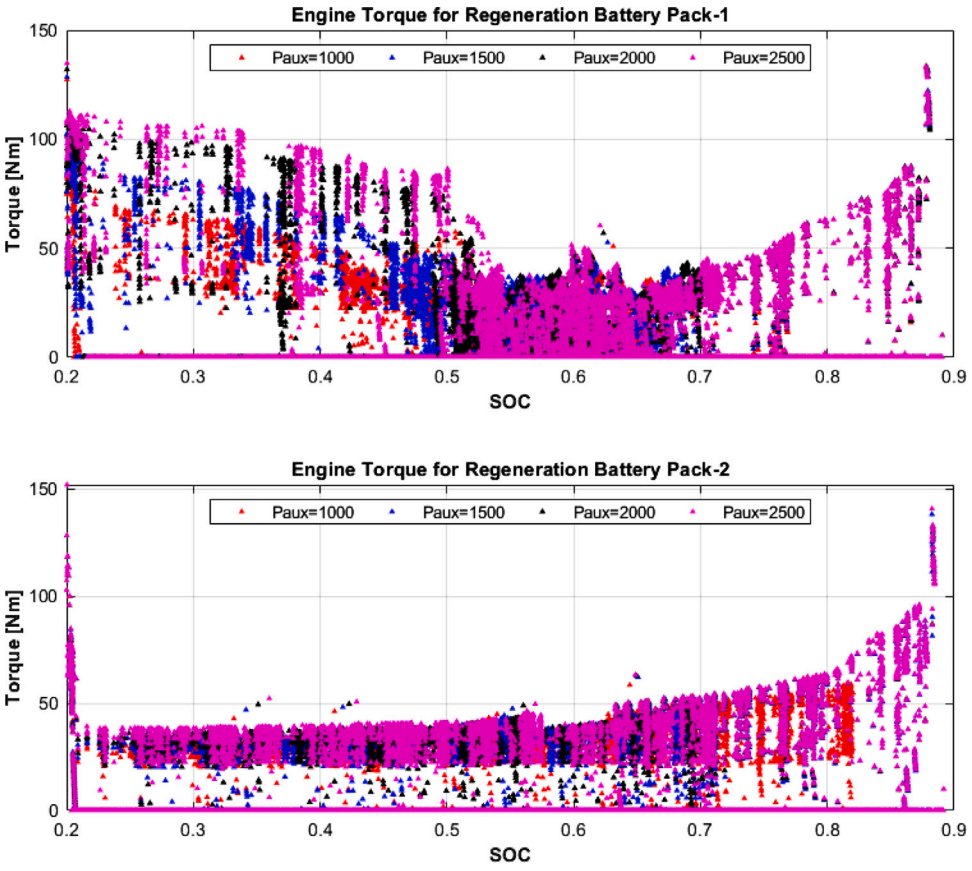

Fig. 17. Additional torque request on engine with respect to SOC.

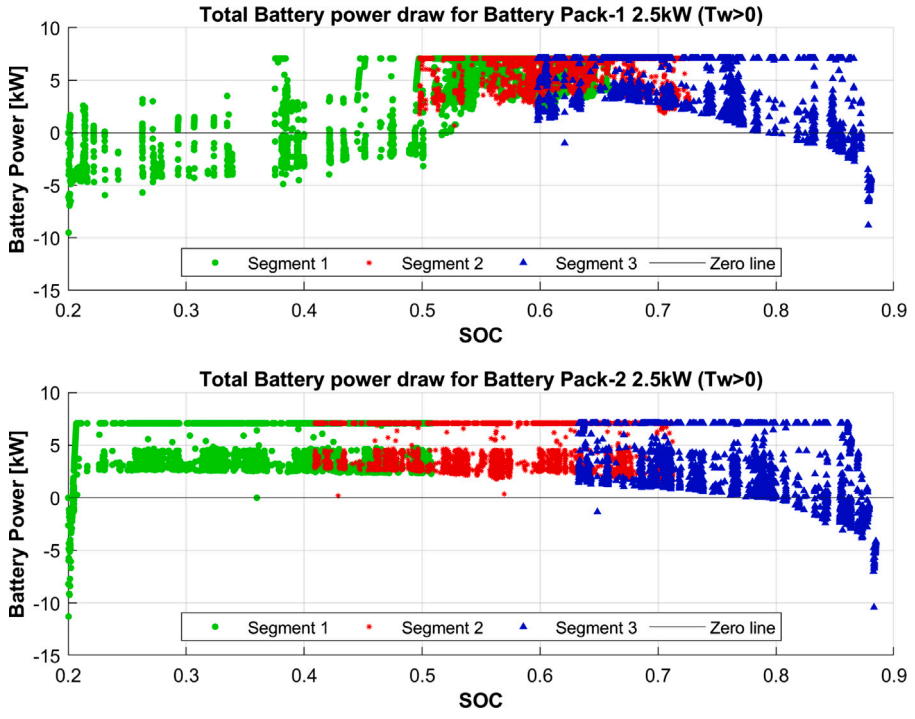

Fig. 18. Battery power for positive torque request.

limitation is immediately apparent: both battery packs, with a 7 kW nominal drive load, cannot exploit the complete EM capacity due to battery current limitations. Theoretically, the battery pack-2 offers an additional regeneration capability of 2.2 kW (approximately) due to increased parallel threads and can therefore operate comparatively closer to the peak power line on the EM map. Also, the speeds of

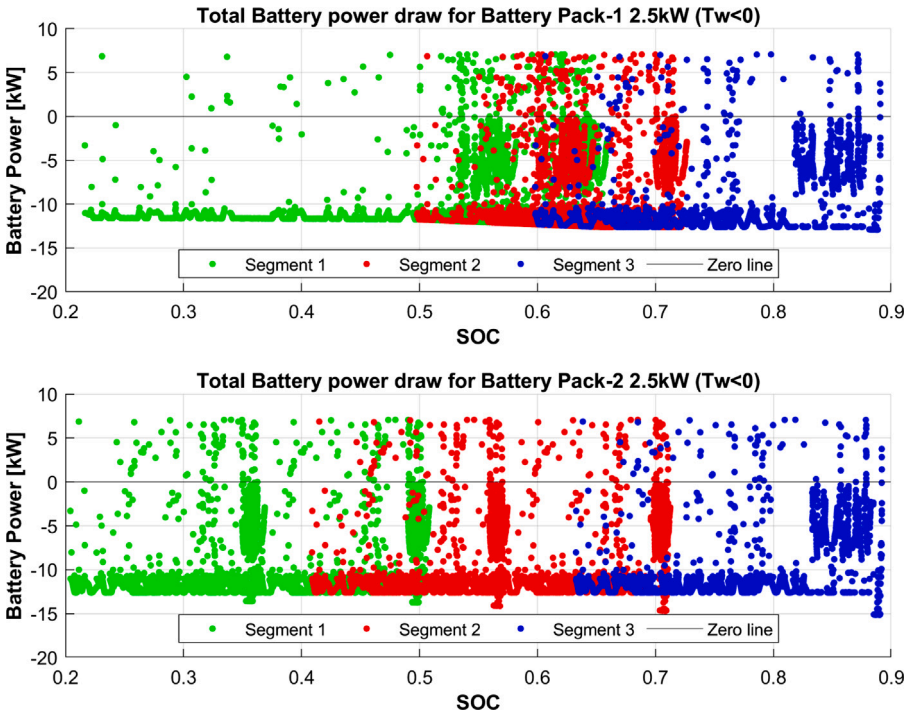

Fig. 19. Battery power for negative torque request.

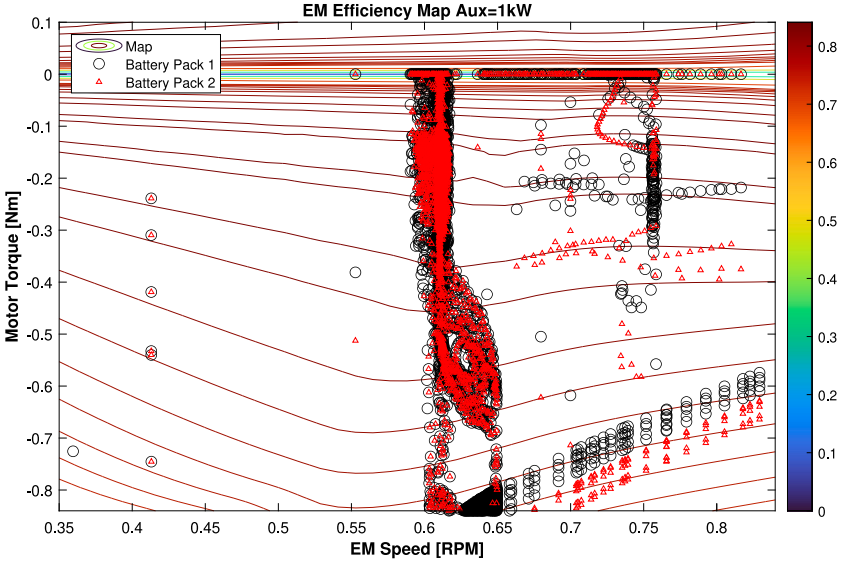

Fig. 20. EM operating points for 1kW nominal auxiliary load.

operation are away from the EM peak efficiency zone and this is a direct consequence of the designed gear ratio between the transmission inlet shaft and EM which is taken to be a constant and not modified in this study. It is theoretically possible to move the points towards high-efficiency zones by increasing this speed ratio.

Fig. 21 shows a similar analysis for a 2.5 kW auxiliary load. In zones under a speed of 0.35, the results are similar for both battery packs as the operating points are coincident. For the battery pack-1, there is a massive increase in operating points between torques of 0 and −0.4 compared to Fig. 20. This is a direct consequence of the limited battery pack capacity and higher requirement for engine-based regeneration to reach the SOC of 90% SOC at the end of the trip.

6.5. Engine efficiency improvement

It is known that parallel hybrid architectures can improve the operating points of the engine, either by increasing torque request at the engine or reducing it through the electric machine. It is understood that low torque regions on the engine map correspond to a low engine efficiency zone throughout the map. These points can be shifted to a higher torque zone which would increase the engine efficiency of the system. To illustrate the effect, the efficiency of engine points from DP results are plotted against the baseline engine efficiency in Figs. 22 and 23.

The DP algorithm selects the correct opportunity for regeneration at the points which correspond to low torque request for traction. When

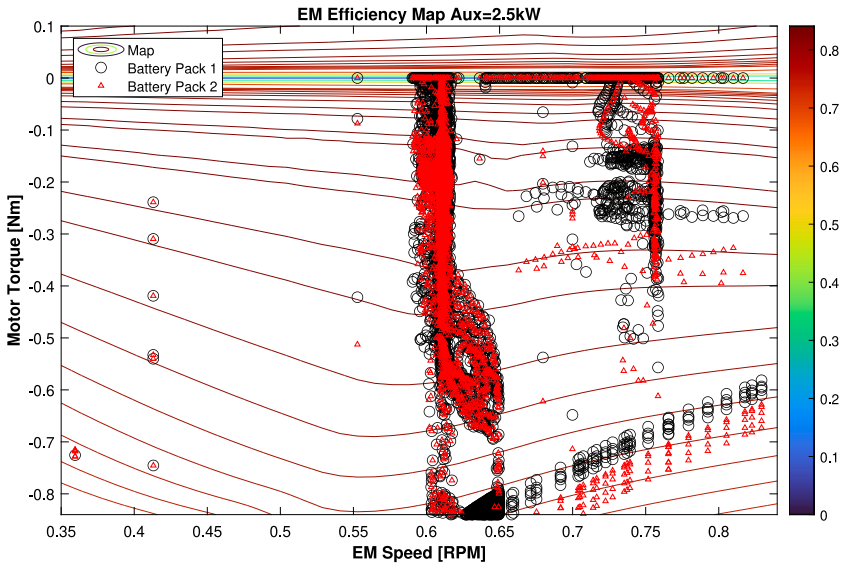

Fig. 21. EM operating points for 2.5 kW nominal auxiliary load.

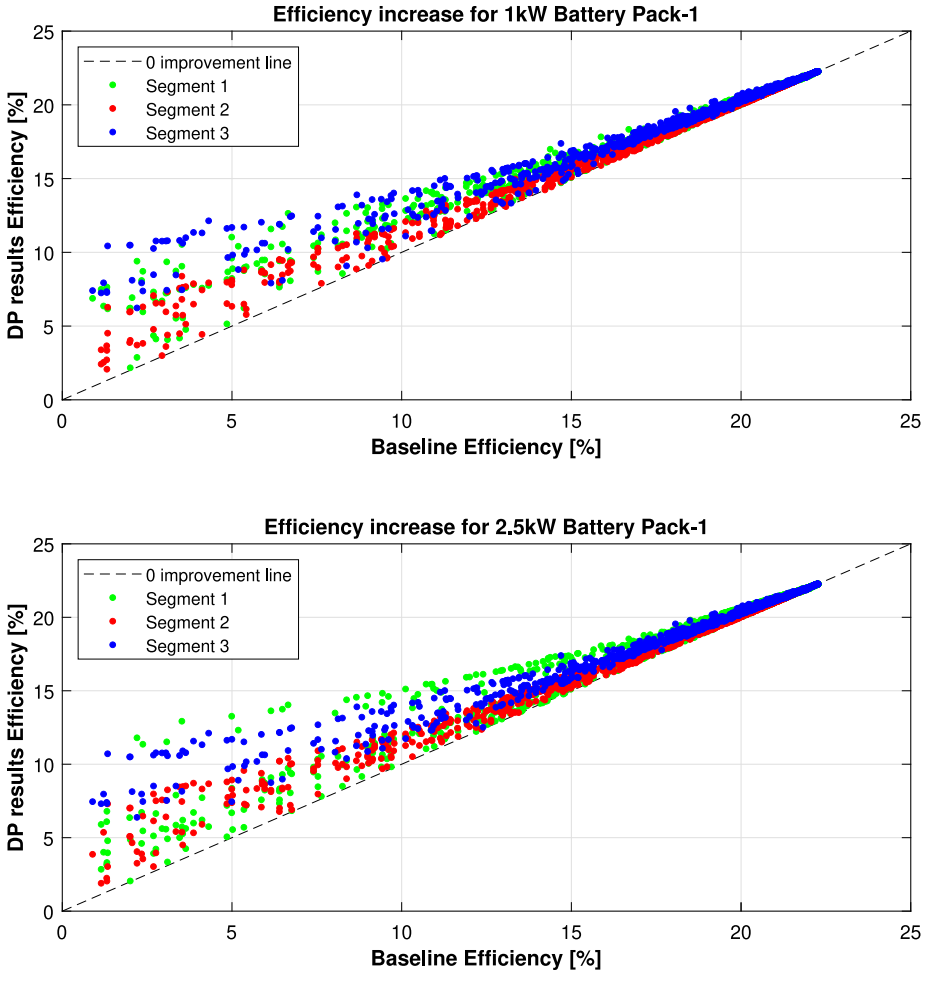

Fig. 22. Engine efficiency improvement for battery pack 1.

these points are shifted towards peak torque zones, the overall efficiency of the system improves and in result further fuel savings is possible. Mostly, the points with the lowest baseline efficiency are affected and these points offer the maximum scope for efficiency increase.

Figs. 24 and 25 further support this selection process and rationale. These figures highlight that the incremental torque on the engine directed for SOC increase is concentrated in region under 1000N.m and the instances beyond this torque are limited in magnitude and occur-

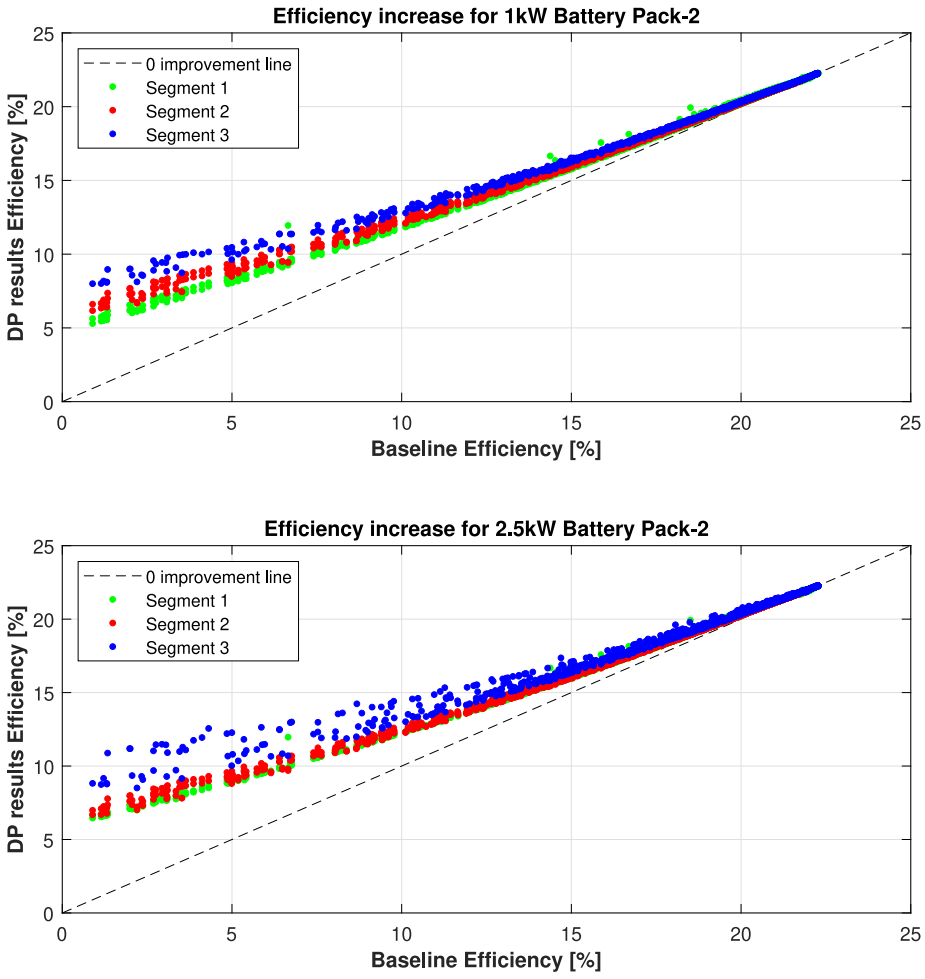

Fig. 23. Engine efficiency improvement for battery pack 2.

Table 1
Fuel consumption comparison for battery pack-1.

Load (kW)	DP (kg)	Mean APU (kg)	Difference (%)	Mean idling (kg)	Difference (%)
1.0	151.64	153.92	1.50	161.00	6.17
1.5	153.77	153.92	0.10	161.00	4.70
2.0	155.89	153.92	−1.26	161.00	3.28
2.5	157.94	153.92	−2.55	161.00	1.94

Table 2
Fuel consumption comparison for battery pack-2.

Load (kW)	DP (kg)	Mean APU (kg)	Difference (%)	Mean idling (kg)	Difference (%)
1.0	151.22	153.92	1.79	161.00	6.47
1.5	152.51	153.92	0.92	161.00	5.57
2.0	154.61	153.92	−0.45	161.00	4.13
2.5	156.69	153.92	−1.77	161.00	2.75

rences. This is because low torque zones are also the low efficiency zones and offer the best opportunity for engine based regeneration since the SOC gain comes at a lower effective fuel cost.

6.6. Fuel consumption comparison

To verify the feasibility of the current solution, average values of fuel consumption from [2] are utilized for APUs based heavy duty truck and idling for a period of 6 hours. The improvements are presented in Tables 1 and 2. Since average power consumption values have not been documented corresponding to the fuel consumption range, the feasibility analysis has used an average value for comparison against DP solution which remains constant for all load cases. Also, a period of only 6 h is used for the idling and APU cases, thus making the benefit estimates from DP conservative. In the absence of detailed power-fuel consumption correlation, such conservative approximations offer a high-level insight for feasibility assessment of hybrid technologies.

It is clear that the advantage ranges from 1.94% to 6.17% for the battery pack-1 against mean idling consumption. These increase to 2.75% to 6.47% for the battery pack-2 respectively. These differences are due to the higher charging limit of the battery pack-2 compared to the battery pack-1. The battery pack-2 can absorb 2kW more at a given instant compared to the battery pack-1 under nominal conditions. APUs however show a better potential for fuel consumption reduction for loads above 1kW for battery pack-1 and 1.5 kW for battery pack-2. Nevertheless, it is a costly investment above the stock vehicle costs and not a direct competition to mild hybrid systems.

7. Analysis using composite "short" cycle based on HHDDT cruise cycle

7.1. Drive cycle and SOC profiles

The drive cycle is based on similar approach as the one presented in the paper. There are three drive segments as described below:

- Segment 1: Composed of 3 repetitions of HHDDT Cruise mode.
- Segment 2: Composed of 3 repetitions of HHDDT Cruise mode.

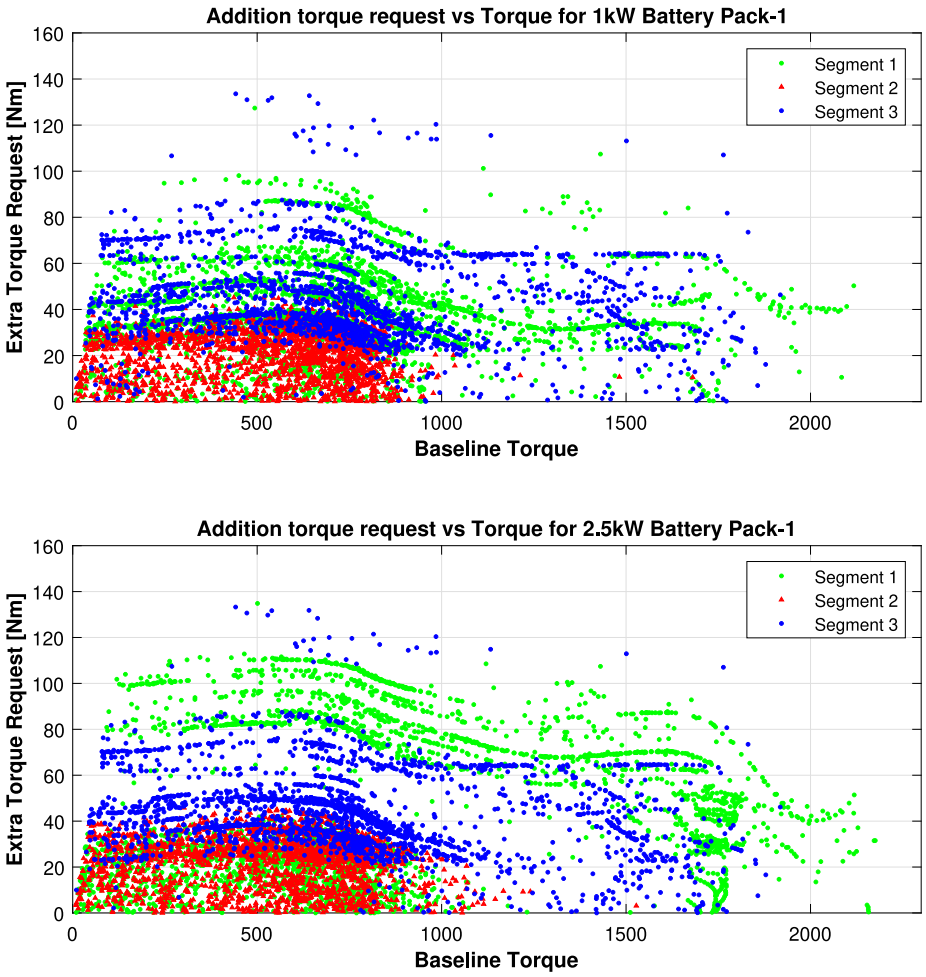

Fig. 24. Incremental torque request on engine with respect to traction torque requirement for battery pack 1.

- Segment 3: Composed of 2 repetitions of HHDDT Cruise mode.

There are two short break periods with the first being between Segment 1 and Segment 2, and the other being between Segment 2 and 3. Segment 3 is followed by a long idle period representing overnight rest of 10 hours. The auxiliary load cycles are synthesized similarly, with a base load of 7kW and varying auxiliary load values during hoteling. Due to a smaller duration of our base cycle, the total distance covered is 296 km and this represents a boundary case where a Class 8 trucks covers a short distance but undergoes similar hoteling periods.

The SOC profile is shown in Fig. 26.

7.2. Engine efficiency enhancement and battery

Similar to results presented in Section 6, the ability to regenerate through the engine assists in improving the engine efficiency throughout the operating range compared to the baseline efficiency is shown in Figs. 27 and 28 for HHDDT drive cycle.

It was seen that the opportunities for regeneration were comparatively limited due to reduced distance and drive times. Hence the energy recovery loss through regeneration was supplemented by added engine operations. This can be clearly seen in Figs. 18, 19, 29 and 30. In the HHDDT cycle, the regeneration is not concentrated between −10 to −15 kW, and the battery regeneration is clearly amplified in positive torque phases in Fig. 29 (the regeneration from engine mode (M3) for three segment over the entire drive cycle) compared to Fig. 18 and in Fig. 30 (the regeneration from braking mode (M3) for three segment over the entire drive cycle)as compared to Fig. 19.

Table 3
Fuel consumption comparison for battery pack-1 HHDDT.

Load (kW)	DP (kg)	Mean APU (kg)	Difference (%)	Mean idling (kg)	Difference (%)
1.0	49.05	49.18	0.25	59.80	17.97
1.5	51.21	49.18	−4.13	59.80	14.36
2.0	53.31	49.18	−8.4	59.80	10.85
2.5	55.38	49.18	−12.61	59.80	7.39

7.3. Fuel consumption for HHDDT based composite cycle

The composite cycle based on HHDDT provides limited opportunities for energy minimization for hoteling; however with a 6 hour idling phase with mean fuel consumption reported in literature, the benefits compared are significant with peak values as high as 18.3%. However, in a “short” long haul cycle the APUs appear to be a better option to minimize overall fuel consumption for any auxiliary load value above 1 kW. It should be noted that these are conservative estimates, and the benefits with drive-train electrification and hoteling loads optimization in real world scenarios will be much more significant even for shorter cycles such as the one presented here based on HHDDT cycle (see Tables 3 and 4).

7.4. Idling efficiency

The idling operating points are determined by the following constraints built into the DP algorithm:

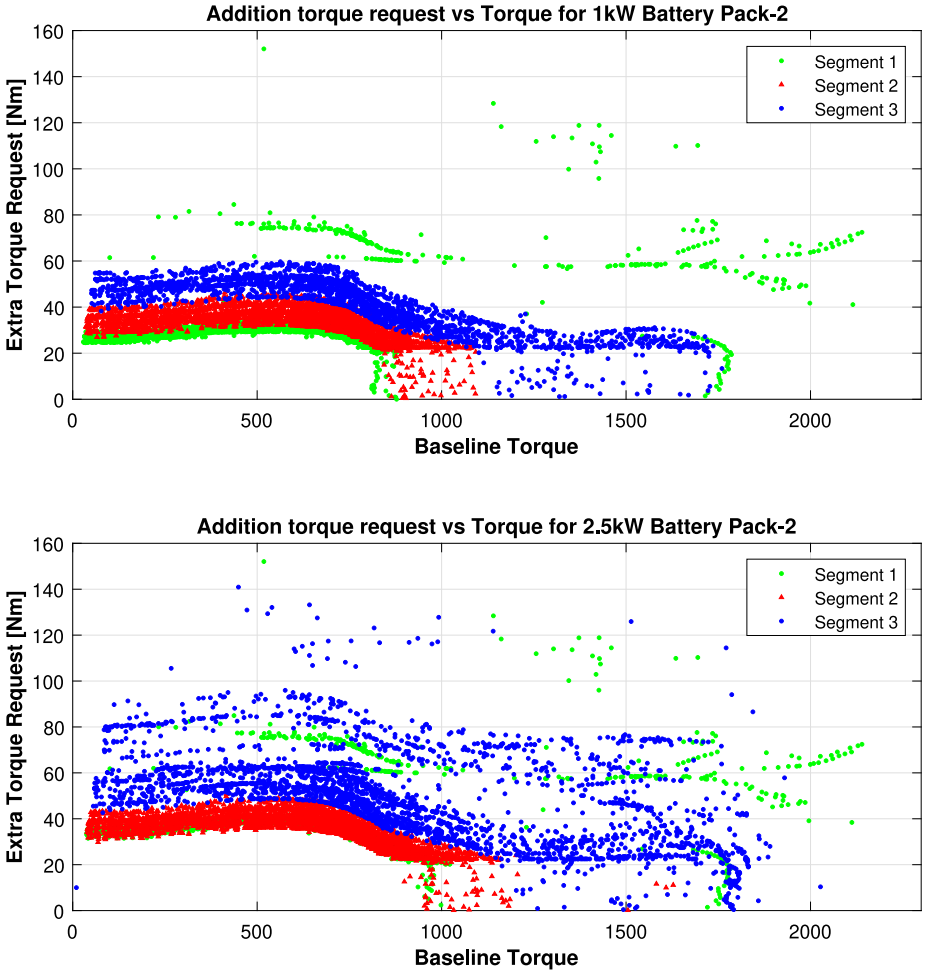

Fig. 25. Incremental torque request on engine with respect to traction torque requirement for battery pack 2.

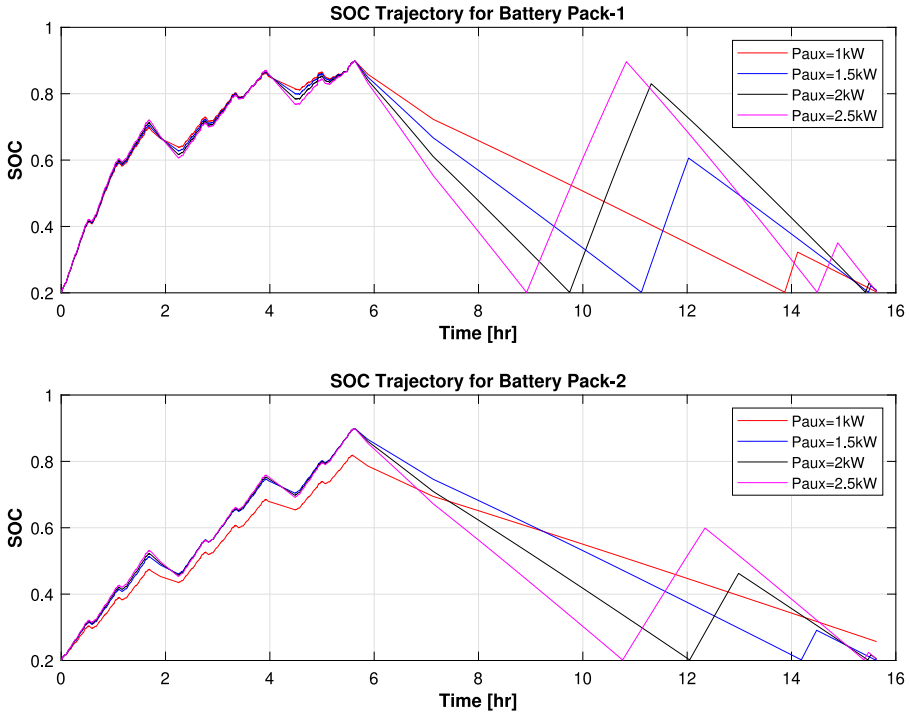

Fig. 26. SOC Profiles for composite cycle based on HHDDT Cycle.

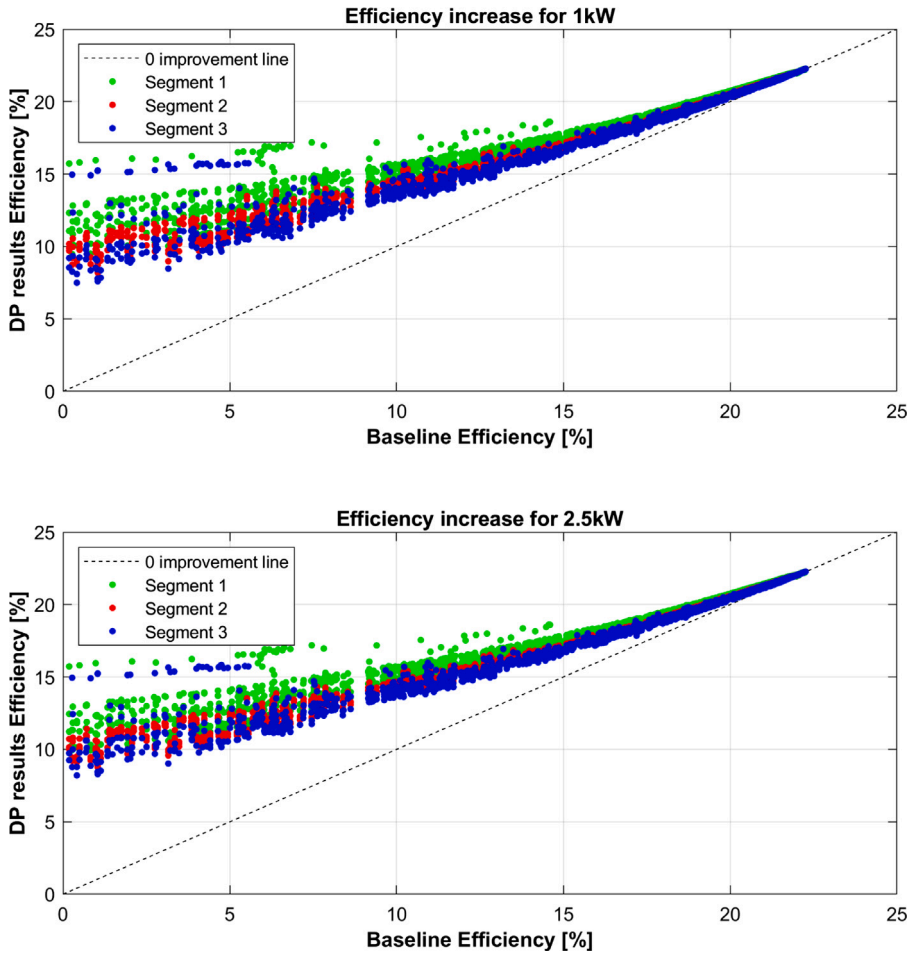

Fig. 27. Engine efficiency improvement for battery pack 1 HHDDT Cycle.

Table 4
Fuel consumption comparison for battery pack-2 HHDDT.

Load (kW)	DP (kg)	Mean APU (kg)	Difference (%)	Mean idling (kg)	Difference (%)
1.0	48.85	49.18	0.66	59.8	18.3
1.5	50.23	49.18	−2.14	59.8	16.00
2.0	52.37	49.18	−6.48	59.8	12.42
2.5	54.46	49.18	−10.73	59.8	8.93

- The engine is allowed to idle only at one particular engine speed during the idling based charging process. This RPM is determined based on manufacturer recommendation and hence the idling based charging takes place at one particular engine and EM RPM as they are mechanically coupled.
- The operating points and number of start stops are determined primarily by the start stop costs imposed during the idling phase. This is because of subjective complaints of recurring start stops with APUs which tend to annoy drivers overnight.

The results showed that during the idling based charging process, the EM and engine operating efficiency are constant at 78.83% and 69.07% of the peak possible overall efficiency, respectively. Also, these values are constant for both the HHDDT based cycle as well as the custom drive cycle. This can be attributed to the following:

- Fig. 31 gives the detail of engine idling mode (M4). While the engine can be operated at a higher efficiency, this compromises the efficiency of the EM operating point due to the nature of the maps as shown in Fig. 31 and hence the algorithm, due to its formulation, is limiting an increase in charging rate. At the charging RPM, the EM efficiency peaks at lower torques while the engine efficiency peaks at higher torques. Since the cost function prioritizes fuel cost over EM efficiency, there is a trade-off with higher compromises on EM efficiency compared to fuel consumption.
- The peak efficiency of the engine cannot be realized at the charging RPM specified as the torques for peak efficiency will violate the peak EM allowed torque. This is due to the nature of the maps and the gear ratio between the EM and engine.
- A similar value across the 2 cycles and multiple auxiliary loads suggest that the start stop cost is limiting the charging rate. If the battery charges faster, there is a possibility to add additional stops which offsets the benefits of the additional engine efficiency.

It is clear that the nature of the maps and the coupling ration between the engine and EM, along with the cost function formulation and start stop costs are determining a limited operation zone during idling-charging.

8. Conclusion

The proposed framework based on DP can serve as a comprehensive tool to evaluate the design feasibility (component sizing) and optimize the powertrain performance (optimal SOC trajectory given the nominal auxiliary loads). The framework is specific to a P2.5 powertrain architecture with the EM operating only in regeneration mode. From a component sizing perspective, it was observed that the limiting factor in energy regeneration is the on board battery pack current limit. Thus,

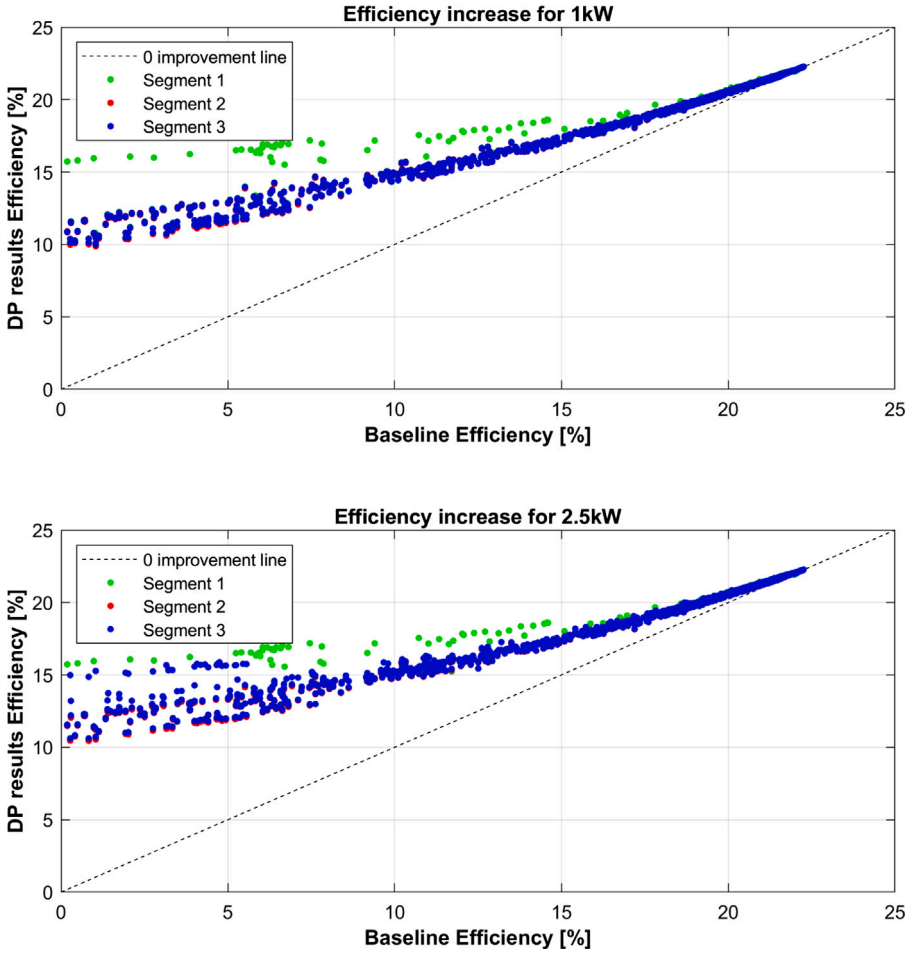

Fig. 28. Engine efficiency improvement for battery pack 2 HHDDT Cycle.

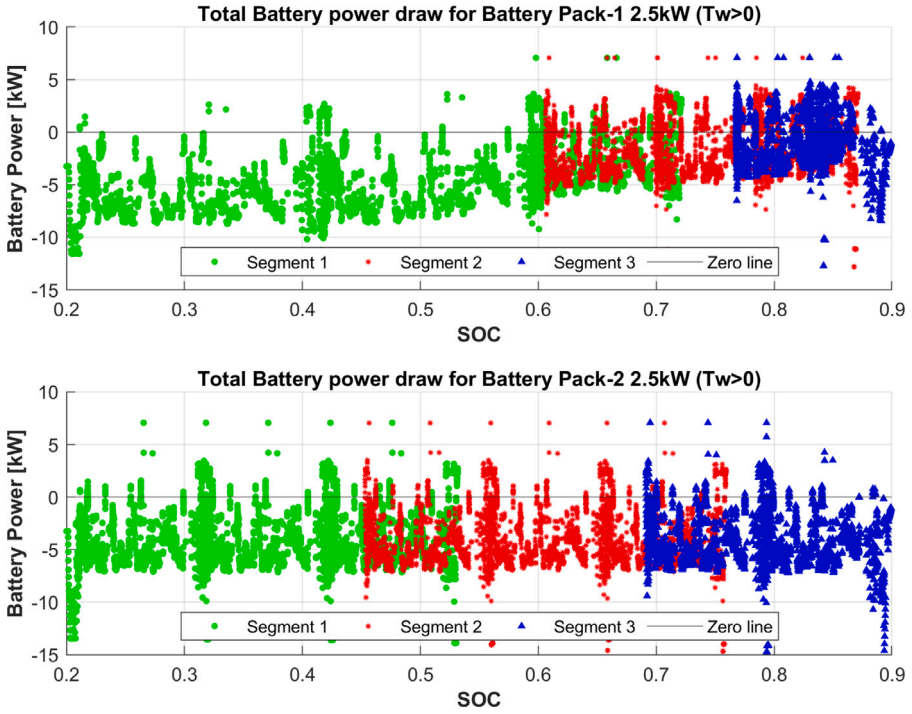

Fig. 29. Battery Power for HHDDT based Cycle during positive wheel torque.

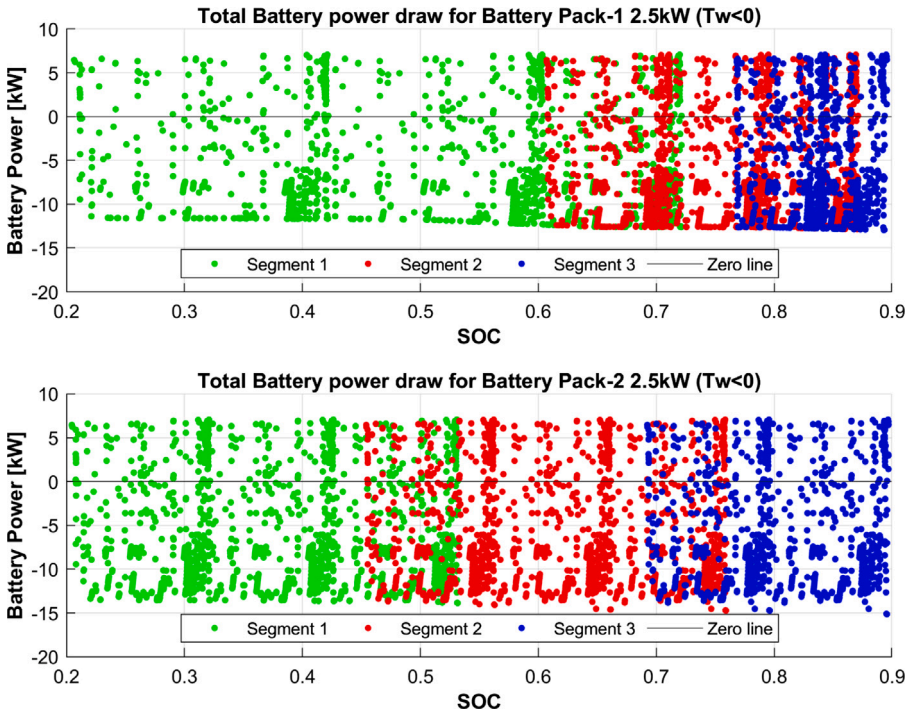

Fig. 30. Battery Power for HHDDT based Cycle during negative wheel torque.

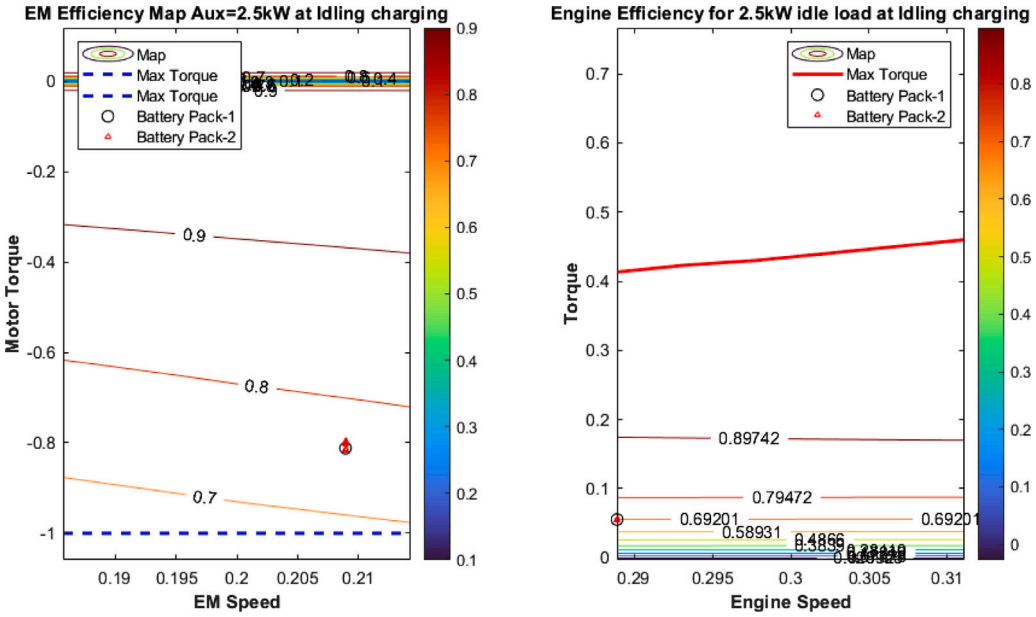

Fig. 31. Normalized Operating points during idling.

the battery pack-2 offers significant improvements compared to the battery pack-1, but is still unable to completely exploit the power limit of the electric machine.

From an optimal control policy perspective, P2.5 architecture is enabled for higher efficiency during all operating conditions and maximum regeneration of energy from the brakes. This contributes to an overall decrease in fuel consumption where hotel operation is supported purely by the onboard battery pack. In terms of feasibility, the solution leads to a maximum of 6.47% fuel consumption reduction with the peak auxiliary load, when compared to an APU-based heavy-duty truck. Although the feasibility estimates are conservative, they can be made more accurate and realistic by developing better methods for a more realistic auxiliary load profile; either through data or by detailed component models.

In future work, the authors are planning to develop the probabilistic models for the hotel loads as a function of weather information, route information and driver preferences.

CRediT authorship contribution statement

Somendra Pratap Singh: Conceptualization, Methodology, Software, Investigation, Visualization, Writing. **Athar Hanif:** Conceptualization, Methodology, Software, Investigation, Visualization, Writing, Supervision. **Qadeer Ahmed:** Conceptualization, Methodology,

Investigation, Writing, Funding acquisition, Supervision. **Maarten Meijer:** Conceptualization, Investigation, Funding acquisition, Supervision. **John Lahti:** Conceptualization, Investigation, Writing.

Data availability

The authors do not have permission to share data.

Acknowledgments

The authors thank the United States Department of Energy for the support for this project. This material is based upon work supported by the Department of Energy, USA, under Grant Number DE-EE0008265.

References

[1] US-DOE. Idle reduction laws and incentives in California. 2019, https://afdc.energy.gov/fuels/laws/IR?state=CA.

[2] ANL. Idling reduction for long-haul trucks: An economic comparison of on-board and wayside technologies. 2012, URL https://publications.anl.gov/anlpubs/2016/10/130502.pdf.

[3] Tran D-D, Vafaeipour M, El Baghdadi M, Barrero R, Van Mierlo J, Hegazy O. Thorough state-of-the-art analysis of electric and hybrid vehicle powertrains: Topologies and integrated energy management strategies. Renew Sustain Energy Rev 2020;119:109596. http://dx.doi.org/10.1016/j.rser.2019.109596.

[4] Yang C, Zha M, Wang W, Liu K, Xiang C. Efficient energy management strategy for hybrid electric vehicles/plug-in hybrid electric vehicles: Review and recent advances under intelligent transportation system. IET Intell Transp Syst 2020;14(7):702–11. http://dx.doi.org/10.1049/iet-its.2019.0606.

[5] Lee H, Park Y, Cha SW. Power management strategy of hybrid electric vehicle using power split ratio line control strategy based on dynamic programming. In: 2015 15th International conference on control, automation and systems. ICCAS, 2015, p. 1739–42. http://dx.doi.org/10.1109/ICCAS.2015.7364645.

[6] Hegde B, Ahmed Q, Rizzoni G. Velocity and energy trajectory prediction of electrified powertrain for look ahead control. Appl Energy 2020;279:115903.

[7] Wu J, Gao B, Zheng Q, Chen H. Optimal equivalence factor calculation based on dynamic programming for hybrid electric vehicle. In: 2017 Chinese automation congress. 2017, p. 6640–5. http://dx.doi.org/10.1109/CAC.2017.8243973.

[8] Jung D, Ahmed Q, Zhang X, Rizzoni G. Mission-based design space exploration for powertrain electrification of series plugin hybrid electric delivery truck. In: SAE technical paper. SAE International; 2018, http://dx.doi.org/10.4271/2018-01-1027.

[9] Tang L, Rizzoni G, Lukas M. Comparison of dynamic programming-based energy management strategies including battery life optimization. In: 2016 International conference on electrical systems for aircraft, railway, ship propulsion and road vehicles international transportation electrification conference. 2016, p. 1–6. http://dx.doi.org/10.1109/ESARS-ITEC.2016.7841430.

[10] Yang Y, Hu X, Pei H, Peng Z. Comparison of power-split and parallel hybrid powertrain architectures with a single electric machine: Dynamic programming approach. Appl Energy 2016;168:683–90.

[11] Dellermann M, Gehring O, Zirn O. Optimal control of energy flow between electrified auxiliaries and powertrain in hybrid-electric heavy-duty vehicles. In: 2020 American control conference. ACC, 2020, p. 4161–8. http://dx.doi.org/10.23919/ACC45564.2020.9147635.

[12] Gao Z, Finney C, Daw C, LaClair TJ, Smith D. Comparative study of hybrid powertrains on fuel saving, emissions, and component energy loss in HD trucks. SAE Int J Commer. Veh 2014;7(2):414–31. http://dx.doi.org/10.4271/2014-01-2326.

[13] Hendricks T, O'Keefe M. Heavy vehicle auxiliary load electrification for the essential power system program: Benefits, tradeoffs, and remaining challenges. In: SAE technical paper. SAE International; 2002, http://dx.doi.org/10.4271/2002-01-3135.

[14] Surampudi B, Redfield J, Ray G, Montemayor A, Walls M, McKee H, et al. Electrification and integration of accessories on a class-8 tractor. In: SAE technical paper. SAE International; 2005, http://dx.doi.org/10.4271/2005-01-0016.

[15] Surampudi B, Walls M, Redfield J, Montemayor A, Ingold C, Abela J. 42-Volt electric air conditioning system commissioning and control for a class-8 tractor. In: SAE technical paper. SAE International; 2004, http://dx.doi.org/10.4271/2004-01-1478.

[16] Redfield J, Surampudi B, Gustavo R, Montemayor A, McKee H, Edwards T, et al. Accessory electrification in class 8 tractors. In: SAE technical paper. SAE International; 2006, http://dx.doi.org/10.4271/2006-01-0215.

[17] Lutsey N, Wallace J, Brodrick CJ, Dwyer HA, Sperling D. Modeling stationary power for heavy-duty trucks: Engine idling vs. Fuel cell APUs. In: SAE Technical Paper. SAE International; 2004, http://dx.doi.org/10.4271/2004-01-1479.

[18] Surampudi B, Redfield J, Montemayor A, Ray G, Ostrowski G, McKee H, et al. Electric air conditioning for class 8 tractors. In: SAE technical paper. SAE International; 2006, http://dx.doi.org/10.4271/2006-01-0165.

[19] Campbell J, Watts W, Kittelson D. Reduction of accessory overdrive and parasitic loading on a parallel electric hybrid city bus. In: SAE technical paper. SAE International; 2012, http://dx.doi.org/10.4271/2012-01-1005.

[20] EATON. US patent - 2019/0265077: Transmission mounted electrical charging system with engine off coasting and dual mode HVAC. 2019.

[21] Zhang B, Zhang J, Xu F, Shen T. Optimal control of power-split hybrid electric powertrains with minimization of energy consumption. Appl Energy 2020;266:114873.

[22] Gao Z, LaClair TJ, Nawaz K, Wu G, Hao P, Boriboonsomsin K, et al. Comprehensive powertrain modeling for heavy-duty applications: A study of plug-in hybrid electric bus. Energy Convers Manage 2022;252:115071.

[23] Tang L, Rizzoni G, Onori S. Energy management strategy for HEVs including battery life optimization. IEEE Trans Transp Electrif 2015;1(3):211–22. http://dx.doi.org/10.1109/TTE.2015.2471180.

[24] Diba F, Esmailzadeh E. A new parallel-series configuration for hybridization of a line-haul truck. In: 2013 IEEE transportation electrification conference and expo. ITEC, 2013, p. 1–6. http://dx.doi.org/10.1109/ITEC.2013.6574525.

[25] Serrao L, Onori S, Sciarretta A, Guezennec Y, Rizzoni G. Optimal energy management of hybrid electric vehicles including battery aging. In: Proceedings of the 2011 American control conference. 2011, p. 2125–30. http://dx.doi.org/10.1109/ACC.2011.5991576.

[26] Onori S, Serrao L, Rizzoni G. Hybrid electric vehicles: Energy management strategies. 2016.